Eddy Viscosity Models for Pure Waves Over Large Roughness Elements

by

Paulo Salles Afonso de Almeida

Submitted to the Department of Civil and Environmental Engineering
in partial fulfillment of the requirements for the degree of

Master of Science in Civil and Environmental Engineering

at the

MASSACHUSETTS INSTITUTE OF TECHNOLOGY
and the
WOODS HOLE OCEANOGRAPHIC INSTITUTION

June 1997

© Massachusetts Institute of Technology 1997. All rights reserved.

Author .....
Department of Civil and Environmental Engineering
March 4, 1997

Certified by .....
Ole S. Madsen
Professor, Department of Civil and Environmental Engineering
Thesis Supervisor

Accepted by .....
Tim Stanton
Chairman, Joint Committee on Applied Ocean Science and Engineering

MASSACHUSETTS INSTITUTE OF TECHNOLOGY

JUN 24 1997 Eng.

Eddy Viscosity Models for Pure Waves Over Large Roughness Elements

by

Paulo Salles Afonso de Almeida

Submitted to the Department of Civil and Environmental Engineering
on March 4, 1997, in partial fulfillment of the
requirements for the degree of
Master of Science in Civil and Environmental Engineering

Abstract

Although the classical Grant and Madsen (1979 and 1986) eddy viscosity model was used successfully to translate wave energy dissipation measurements into an equivalent roughness by Mathisen (1993), it fails to resolve the details of the boundary layer velocity profile. This issue is addressed in the present study, in which three models are presented and their abilities to predict the details of the velocity profile are compared.

First, a constant eddy viscosity model for wave boundary layer flows over two-dimensional roughness elements simulating wave-generated, fully developed ripples is presented. Mathisen's (1993) measurements of energy dissipation for periodic waves over artificial bedforms are interpreted in terms of drag resistance, and a good correlation is obtained for the drag coefficient . C_D, and the ratio of the ripple height, η, to the maximum bottom excursion amplitude, A_b. This dependence of C_D on η/A_b is shown to be in general agreement with Sarpkaya's (1981) analysis of the drag coefficient as a function of the Keulegan-Carpenter number. The drag law dissipation is similar in nature to that obtained for a constant eddy viscosity wave boundary layer model with $\nu_t \propto \eta^4/(\lambda^2 T)$, where λ is the ripple length and T is the wave period. This eddy viscosity, as function of the inverse of the wave period, was also obtained by Sleath (1991). However, here the eddy viscosity is also a function of the ripple steepness (height and length), and not of any other flow parameter. The constant eddy viscosity model is applied with the linearized boundary layer equation to predict detailed velocity profiles (magnitudes and phases) and compare favorably with measurements from Mathisen (1993) and Barrantes (1996). The results of this study support the use of a constant eddy viscosity for the prediction of energy dissipation as well as the details of the velocity profile within the wave boundary layer for flows over rippled beds.

Then a model based entirely on the classical GM model is presented, in which the no-slip condition is modified to be at the bottom and not at $z = z_0$. With this change

the predicted velocity profile agrees significantly better with the measurements than does the original model. Moreover, the analysis of the theoretical boundary layer thickness shows that the latter is proportional to the product of two monotonically increasing functions of the relative roughness, and not only of the boundary layer scale l, as thought before. However, some features of the profile are not described accurately and this becomes the motivation to develop a model consisting of a combination of the first two.

In the combined model the eddy viscosity is considered linearly varying with depth in the lower portion of the boundary layer and then constant above that. This model appears to describe the details of the velocity profile with the same accuracy as the constant eddy viscosity model. Additionally, its prediction of the energy dissipation, given a prescribed bottom roughness proportional to the ripple height, turns out to be in slightly better agreement with experiments performed over a rippled movable bed, than the predictions using the Constant eddy viscosity model.

Thesis Supervisor: Ole S. Madsen
Title: Professor, Department of Civil and Environmental Engineering

Acknowledgments

First of all I would like to thank my advisor, Professor Ole Madsen, for all his support throughout this period of my graduate studies. His lectures, his insight and his way of approaching the physical problems were always for me a motivation to pursue and accomplish this project. Besides, since I came here, his friendship, his interest and his concern for any non-academic problem that might arise helped me to have an easier adaptation to this new rhythm of life.

I am also grateful to my co-advisor at WHOI, Dr. John Trowbridge, who showed me other aspects of the beauty of the coastal hydrodynamics and helped me in my first steps with Matlab. I would also like to thank my mentors in the Engineering Institute in Mexico, Victor Franco, Jesús Gracia and Oscar Fuentes, for their motivating support and their belief in me. I am indebted to the National Autonomous University of Mexico for its financial support, making possible this venture. My sincerest appreciation to all the people in Parsons Lab for their friendship.

Finally, I would like to thank my wife, Irina, for all her unconditional support, her patience and her love.

To Irina and Paloma,

who deserve all the time I spent writing this work.

Contents

1 Introduction **14**

1.1 Introduction 14

1.2 Motivation 18

1.3 Outline 21

2 Drag Model **23**

2.1 A Simple Drag Coefficient Relationship 23

2.2 Experimental Data 27

2.3 Analogy with the Keulegan-Carpenter Number 30

3 Constant Eddy Viscosity Model **34**

3.1 Experimental Data 34

3.2 Comparison with Sleath's Constant Eddy Viscosity Model 36

3.3 Velocity Profile Prediction 41

4 Modified Grant-Madsen Model **43**

4.1 Theoretical Formulation 43

4.1.1 Velocity Solution 43

4.1.2 Closure 45

4.2 Velocity Profile Prediction 47

4.2.1 Comparison of the Velocity Profile Predictions 47

4.2.2 Comparison of Boundary Layer Thickness Predictions 49

5 Combined Model **56**

5.1 Theoretical Formulation 57

5.2 Closure 59

5.3 Velocity Profile and Boundary Layer Thickness Predictions 62

6 Energy Dissipation Factor and Bottom Roughness Analysis **65**

6.1 Performance of the Constant ν_t Model 66

6.2 Performance of the Combined Model 69

7 Conclusions **75**

A Velocity Profiles **79**

B Movable Bed Data **85**

C Details of the Energy Dissipation Factor Non-linear Regression **93**

List of Figures

1-1 Flow over a bottom consisting of large roughness elements. 19

2-1 Separation and eddy formation downstream a standard artificial ripple. . . 24

2-2 Total force experienced by the bedform, F, and bottom velocity $\tilde{u}_b$ as a function of time. Both functions have been normalized as $F' = F/F_{max}$ (*circles*) and $\tilde{u}'_b = \tilde{u}_b/u_b$ (*solid line*). 25

2-3 Ratio of the ripple height over the bottom excursion amplitude, η/A_b, as a function of the drag coefficient, C_D. Experimental values (*circles*) and linear fitting (*solid line*). The coefficient of determination is $r^2 = 0.87$. . . 28

2-4 Slope C_{D_0} for 100 sets of simulated η/A_b. The three horizontal lines are the mean slope (*solid line*) and the 66% confidence interval (*dashed lines*). . . 29

2-5 Analogy between flow over a cylinder and flow over a ripple. 31

2-6 Drag coefficient as a function of the Keulegan-Carpenter number. Sarpkaya's experimental results (*circles and dashed line*); Mathisen's (1993) experimental results (*stars*). 32

3-1 Eddy Viscosity ν_t as a function of $\eta^4/(\lambda^2 T)$. Both quantities are in $(cm^2.s^{-1})$. Experimental values obtained from Equation (3.3)(*crosses*) and linear fitting (*solid line*). The coefficient of determination is $r^2 = 0.91$. 35

3-2 Comparison between Sleath's (1991) model and the Constant eddy viscosity model presented here using data from Sleath (1985) and Mathisen (1993). **(a)** ν_t as a function of $\eta^4/(\lambda^2 T)$ using Mathisen's data; $r^2 = 0.91$. **(b)** ν_t as a function of $(A_b^{3/2}\eta^{1/2})/T$ using Mathisen's data; $r^2 = 0$. **(c)** ν_t as a function of $(A_b^{3/2}\eta^{1/2})/T$ using Sleath's data; $r^2 = 0.73$. **(d)** ν_t as a function of $\eta^4/(\lambda^2 T)$ using Sleath's data; $r^2 = 0.19$. Experimental values (*crosses*) and linear fittings (*solid lines*). The circled data points in (a) and (b) correspond to the experiments with $\lambda = 20cm$. All the axis have the unit of $cm^2.s^{-1}$. 39

3-3 Velocity profiles obtained from 1) the classical Grant-Madsen eddy viscosity model (*dotted line*), 2) the Constant eddy viscosity model presented here (*dash-dotted line*), and 3) Mathisen's Experiment "a" measurements above the trough of the ripples (*pluses*) and above the crest of the ripples (*circles*). The input parameters for the models corresponding to experiment "a" are shown in Table 2.1. The GM model needs the additional information of the bottom roughness magnitude, which is shown in Table 4.1. 42

4-1 Velocity profiles obtained from 1) the Modified Grant-Madsen eddy viscosity model (*dotted line*), 2) the Constant eddy viscosity model presented in Chapter 3 (*dash-dotted line*), and 3) Mathisen's Experiment "a" measurements above the trough of the ripples (*pluses*) and above the crest of the ripples (*circles*). 48

4-2 Constant $\mathcal{A}$, from Equation (4.17), as a function of A_b/k_N, for different approximations of $|u_d|$ to u_b: 1) 1 % of u_b (*pluses*), 2) 5 % of u_b (*circles*), and 3) 10 % of u_b (*crosses*). 54

5-1 Velocity amplitude profiles obtained from 1) the Constant eddy viscosity model presented in Chapter 3 (*dash-dotted line*), 2) the Modified Grant-Madsen eddy viscosity model presented in Chapter 4(*dotted line*), 3) the Combined eddy viscosity model presented here, for different values of α_m (*solid lines*). 60

5-2 Velocity profiles obtained from 1) the Constant eddy viscosity model presented in Chapter 3 (*dash-dotted line*), 2) the Modified Grant-Madsen eddy viscosity model presented in Chapter 4(*dotted line*), 3) the Combined eddy viscosity model presented here, with $\alpha_m = 0.5$ (*solid line*) and, 4) Mathisen's Experiment "a" measurements above the trough of the ripples (*pluses*) and above the crest of the ripples (*circles*). 62

6-1 Eddy Viscosity ν_t as a function of $\eta^4/(\lambda^2 T)$. Both quantities are in $(cm^2.s^{-1})$. Experimental data from Carstens, Neilson and Altimbilek (1969)(*pluses*), Lofquist (1986)(*circles*), Rosengaus (1987) and Mathisen (1989)(*crosses*). The linear fitting (*solid line*) has a coefficient of determination $r^2 = 0.70$. . 68

6-2 Measured and predicted energy dissipation factors, as a function of the relative roughness, A_b/k_N. Theoretical values using Equation (6.6) with $k_N = 12.3$ (*solid line*); data from Carstens et al. (1969) (*pluses*); data from Lofquist (1986) (*circles*); data from Rosengaus (1987) and Mathisen (1989) (*crosses*). 74

A-1 Velocity profiles obtained from 1) the Constant eddy viscosity model presented in Chapter 3 (*dash-dotted line*), 2) the Modified Grant-Madsen eddy viscosity model presented in Chapter 4(*dotted line*), 3) the Combined eddy viscosity model presented here (*solid line*)and, 4) Mathisen's Experiment "a" measurements above the trough of the ripples (*pluses*) and above the crest of the ripples (*circles*). 80

A-2 Velocity profiles obtained from 1) the Constant eddy viscosity model presented in Chapter 3 (*dash-dotted line*), 2) the Modified Grant-Madsen eddy viscosity model presented in Chapter 4(*dotted line*), 3) the Combined eddy viscosity model presented here (*solid line*)and, 4) Mathisen's Experiment "b" measurements above the trough of the ripples (*pluses*) and above the crest of the ripples (*circles*). 81

A-3 Velocity profiles obtained from 1) the Constant eddy viscosity model presented in Chapter 3 (*dash-dotted line*), 2) the Modified Grant-Madsen eddy viscosity model presented in Chapter 4(*dotted line*), 3) the Combined eddy viscosity model presented here (*solid line*)and, 4) Mathisen's Experiment "c" measurements above the trough of the ripples (*pluses*) and above the crest of the ripples (*circles*). 82

A-4 Velocity profiles obtained from 1) the Constant eddy viscosity model presented in Chapter 3 (*dash-dotted line*), 2) the Modified Grant-Madsen eddy viscosity model presented in Chapter 4(*dotted line*), 3) the Combined eddy viscosity model presented here (*solid line*)and, 4) Mathisen's Experiment "n" measurements above the trough of the ripples (*pluses*) and above the crest of the ripples (*circles*). 83

A-5 Velocity profiles obtained from 1) the Constant eddy viscosity model presented in Chapter 3 (*dash-dotted line*), 2) the Modified Grant-Madsen eddy viscosity model presented in Chapter 4(*dotted line*), 3) the Combined eddy viscosity model presented here (*solid line*)and, 4) Barrantes' Experiment "PW0" measurements above the trough of the ripples (*pluses*) and above the crest of the ripples (*circles*). 84

List of Tables

2.1 Artificial Bedform Data from Mathisen (1993) 27

2.2 Drag Coefficient and wave parameters for each experiment. 28

4.1 Bottom roughness k_N, obtained from Mathisen's (1993) and Barrantes' (1996) experiments, using the Modified GM model. 47

4.2 Boundary layer thickness predictions using the Constant ν_t model and the Modified GM model. All the values are in cm. 53

4.3 Constant $\mathcal{A}$, from Equation (4.17), as a function of A_b/k_N, for different approximations of $|u_d|$ to u_b. 54

5.1 Bottom roughness k_N, obtained from Mathisen's (1993) and Barrantes' (1996) experiments, using the Combined model. 61

5.2 Boundary layer thickness predictions using the Constant ν_t model and the Combined model. All the values are in cm. 64

6.1 Values of the constant of proportionality $\mathcal{C}$ for Equation (6.4) using data from Carstens et al. (1969), Ca.; Lofquist (1986), Lo.; Rosengaus (1987), Ro.; and Mathisen (1989), Ma. 67

6.2 Statistics of the ratio of the measured and the theoretical f_e, using fixed bed data from Mathisen (1993) and movable bed data from Carstens et al. (1969), Ca.; Lofquist (1986), Lo.; Rosengaus (1987), Ro.; and Mathisen (1989), Ma. 69

6.3 Values of α and β and statistics of the ratio of the measured and the theoretical f_e. The data used is the fixed bed data from Mathisen (1993) and the movable bed data from Carstens et al. (1969), Ca.; Lofquist (1986), Lo.; Rosengaus (1987), Ro.; and Mathisen (1989), Ma. 71

B.1 Carstens et al. (1969).Wave tunnel data on ripple geometry and energy dissipation under regular waves. 86

B.2 Lofquist (1986). Wave tunnel data on ripple geometry and energy dissipation over equilibrium ripples with regular waves. Bed characteristics: $d_{50} = 0.18mm$ and $s = 2.65$. 87

B.3 Lofquist (1986). Wave tunnel data on ripple geometry and energy dissipation over equilibrium ripples with regular waves. Bed characteristics: $d_{50} = 0.55mm$ and $s = 2.65$. 88

B.4 Lofquist (1986). Continuation of Table B.3. 89

B.5 Lofquist (1986). Wave tunnel data on ripple geometry and energy dissipation over growing ripples with regular waves. Bed characteristics: $d_{50} = 0.18mm$ and $s = 2.65$ for the first section of the table and $d_{50} = 0.55mm$ and $s = 2.65$ for the second section. 90

B.6 Rosengaus (1987). Wave flume data on ripple geometry and energy dissipation over sandy bottom. 91

B.7 Mathisen (1989). Wave flume data on ripple geometry and energy dissipation over sandy bottom. 92

Chapter 1

Introduction

1.1 Introduction

In coastal regions, understanding the interaction between ocean and land is fundamental in relation to several engineering topics and in general for a sustainable relationship between humans and nature. In this sense, one of the most important processes is the sediment transport on the continental shelf, which affects not only the beach and coastline morphodynamics, but also waterways operations and the stability of coastal structures.

Sediment transport is due to waves and currents, which are the events that commonly dominate the coastal hydrodynamic environment. Indeed, as wind waves travel from deep water to the coast, entering the continental shelf, they feel the effect of the bottom as well as the bottom feels the effect of the waves, and both transform accordingly. The transformations to the flow due to the bottom include refraction, diffraction, shoaling, and bottom frictional energy losses. Transformations of the bottom due to the flow are related to its mobility; in fact, the bottom usually consists of sediment which is moved by the waves and currents. More precisely the waves, with their back and forth movement, suspend the sediment grains, making them available to be transported by the current.

An accurate model of sediment transport depends on a proper representation of the fluid velocity field associated with the waves and currents. In nature, the flow is turbulent and takes place over an irregular, and often movable bed of varying permeability. Therefore, many simplifying assumptions must be made in order to be able to treat the problem mathematically.

With respect to the flow, the first simplification is to describe it by its harmonic components. Some work has been done to describe some of the relevant aspects of the flow-bottom interaction using a spectral representation of the flow (*e.g.*, Madsen, Poon and Graber, 1988; and Madsen, 1994) and some experiments have been performed (*e.g.*, Rosengaus, 1987; Mathisen, 1989 and 1993; and Barrantes, 1996). However, this picture is often considerably simplified in the majority of the sediment transport related studies. For example, when faced with flow modeling in laboratory experiments, the currents are considered as quasi steady flows and the waves as monochromatic with height H and radian frequency ω.

Throughout most of the depth of the water, the main body of fluid motion can be considered nearly irrotational and can typically be described by potential flow theory. The viscous effects are usually concentrated in thin layers near the boundaries. Indeed, at the bottom, a "no-slip" boundary condition exists, i.e., the velocity is equal to zero. Therefore, near the bottom, a relatively thin region exists, called the *bottom boundary layer*, in which the velocity varies from zero to the velocity prescribed by the potential flow solution. In this region, the effects of viscosity are important and potential flow theory does not apply.

Although natural flows tend to be turbulent, it is worthwhile to base the analysis on the classical theory of laminar flow over a smooth bed because many of its features are present in natural flows. The general equations of motion are the Navier-Stokes equations. In the case of the bottom boundary layer under unidirectional waves, only the equation for the x-component of the flow is considered, which reads (see, *e.g.*, Le

Méhauté, 1976, pp 59–66)

$$\frac{\partial \tilde{u}}{\partial t} + \tilde{u}\frac{\partial \tilde{u}}{\partial x} + \tilde{w}\frac{\partial \tilde{u}}{\partial z} = -\frac{1}{\rho}\frac{\partial p}{\partial x} + \nu\frac{\partial^2 \tilde{u}}{\partial z^2}, \tag{1.1}$$

where $\tilde{u}$ and $\tilde{w}$ are the wave velocities in the x and z directions, respectively, ρ is the fluid density, p is the pressure, and ν is the kinematic viscosity of the fluid.

Assuming the non-linear convective acceleration terms to be small, i.e. equivalent to linear wave theory, the equation of motion becomes

$$\rho\frac{\partial \tilde{u}}{\partial t} = -\frac{\partial p}{\partial x} + \frac{\partial \tau}{\partial z}, \tag{1.2}$$

where τ is the viscous shear stress defined by $\tau = \rho\nu\, du/dz$.

This equation of motion can be further simplified under the assumption of hydrostatic pressure distribution within the boundary layer, that is, when the vertical accelerations are negligible compared to the acceleration of gravity. Then we can use the fact that the shear stresses vanish outside the boundary layer so that

$$\rho\frac{\partial \tilde{u}_b}{\partial t} = -\frac{\partial p}{\partial x}, \tag{1.3}$$

where $\tilde{u}_b$ is the velocity just outside the boundary layer. Then we can rewrite Equation (1.2) in the form

$$\rho\frac{\partial}{\partial t}(\tilde{u} - \tilde{u}_b) = \frac{\partial \tau}{\partial z}. \tag{1.4}$$

For laminar flow the shear stress is simply the viscous shear stress defined above, i.e.

$$\tau = \rho\nu\frac{\partial \tilde{u}}{\partial z}. \tag{1.5}$$

So, the equation of motion can be written as

$$\frac{\partial}{\partial t}(\tilde{u} - \tilde{u}_b) = \nu\frac{\partial^2}{\partial z^2}(\tilde{u} - \tilde{u}_b). \tag{1.6}$$

With the definition of the tilde notation being the real part of

$$\tilde{u}_i = u_i \, \mathrm{e}^{i(\omega t - kx)}, \tag{1.7}$$

it can easily be shown that the solution of this equation, given the boundary conditions $u \to u_b$ as $z \to \infty$ and $u = 0$ at $z = 0$, is

$$\tilde{u} = u_b(1 - \mathrm{e}^{-(1+i)z/\delta_{lam}})\mathrm{e}^{\mathrm{i}(\omega \mathrm{t} - \mathrm{kx})}, \tag{1.8}$$

in which

$$\delta_{lam} = \sqrt{\frac{2\nu}{\omega}}, \tag{1.9}$$

and, according to linear wave theory, $u_b = (a\omega)/(\sinh kh)$, where k is the wave number, a the wave amplitude and h the depth. This shows that the velocity within the boundary layer approaches u_b exponentially away from the bed, with a decay length scale of δ_{lam}. It is customary to use this parameter to define the thickness of the laminar boundary layer.

From Equations (1.5) and (1.8), the bottom shear stress is given by

$$\tau_b = \rho\nu \left.\frac{\partial \tilde{u}}{\partial z}\right|_{z=0} = \rho\nu\sqrt{2}\frac{u_b}{\delta_{lam}} = \rho u_b \sqrt{\nu\omega} \, \mathrm{e}^{\mathrm{i}(\frac{\pi}{4} + \omega \mathrm{t} - \mathrm{kx})}. \tag{1.10}$$

This shows in turn that there is a phase shift of $\frac{\pi}{4}$ between the bottom shear stress and the outer flow velocity and that the maximum bottom shear stress is proportional to u_b and inversely proportional to δ_{lam}. With the definition

$$\tau_{b,max} = \frac{1}{2}\rho f_w u_b^2 \tag{1.11}$$

from Jonsson (1966), the wave friction factor for smooth, laminar flow is

$$f_{w,lam} = \frac{2}{\sqrt{\Re e}}, \tag{1.12}$$

where $\Re e = \frac{A_b^2 \omega}{\nu}$ is the Reynolds number and A_b is the bottom excursion amplitude.

Finally, the time-averaged rate of energy dissipation due to bottom friction is given, as obtained by Kajiura (1968), by

$$E_d = \overline{\tau_b \tilde{u}_b}, \tag{1.13}$$

where the overbar indicates a time average over one period of the oscillatory motion. For laminar flow, using Equations (1.7) and (1.10) this leads to

$$E_d = \frac{\sqrt{2}}{4} \rho \sqrt{\nu \omega}\, u_b^2 \tag{1.14}$$

1.2 Motivation

When dealing with sediment transport modeling, the most important part of the flow is the bottom boundary layer through which the main flow influences the bed. From the opposite point of view, i.e., when dealing with flow dynamics, the bottom boundary layer is intuitively defined as the layer inside which the flow is significantly influenced by the bed.

Additionally, the vertical extent or thickness of the boundary layer indicates the extent of upward diffusion of viscous effects into the flow stream. As seen in Equation (1.9) for the laminar case, it has been noticed that the boundary layer thickness, δ is of the form

$$\delta \propto \sqrt{\nu_t T}, \tag{1.15}$$

where ν_t is the eddy viscosity and T is the flow period.

Given the difference between typical periods of oscillation of currents and waves, the wave bottom boundary layer will be much thinner than the one generated by the current, as seen in Figure 1-1. Since thinner boundary layers mean steeper velocity gradients and therefore larger shear stresses for a certain free stream velocity, the

waves will tend to dominate over the currents with respect to the shear stress they induce on the bottom.

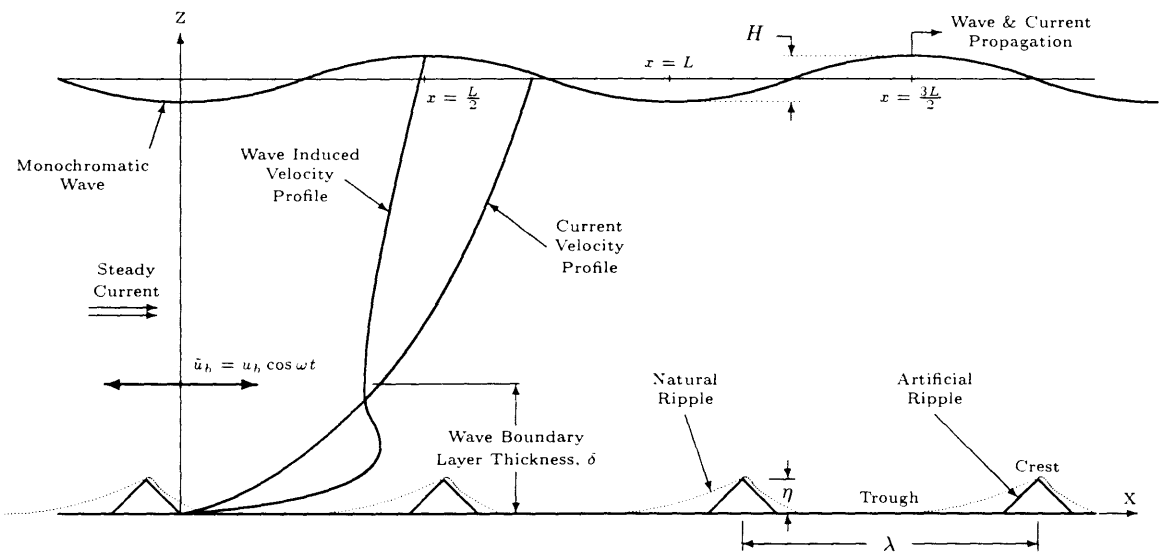

Figure 1-1: Flow over a bottom consisting of large roughness elements.

This steep velocity gradient within the wave bottom boundary layer produces high shear stresses and turbulent flows, which affect the bottom significantly by suspending the sediments and eventually forming bottom bedforms. Those bedforms, in turn, increase fluid shear and enhance energy dissipation. For the purpose of estimating the amount of sediment that can be made available for transport, the focus must then be on the *wave* bottom boundary layer.

It is therefore important to obtain a reasonably accurate estimate of, and be able to predict, both the shear stress intensity and the boundary layer thickness. Since we lack a detailed description of the flow in the boundary layer because of its inherently turbulent behavior, the studies performed so far have been mostly experimental, borrowing concepts from river flows like the friction factor and the equivalent roughness concepts. Several theoretical models for turbulent bottom boundary layers have also been proposed: *quasi-steady* models which assume that the velocity distribution is at all times logarithmic throughout the boundary layer; *velocity distribution* models

which seek empirical expressions for the velocity, in analogy with smooth, laminar oscillatory flow; *eddy viscosity* models which replace the kinematic viscosity by an a priori unknown eddy viscosity; and the *one-equation* and *two-equation* models which try to improve the description of the vertical distribution of turbulence. A more detailed description of these models can be found in Fredsøe and Deigaard (1992) and Nielsen (1992).

Nevertheless, it has been noticed that the prediction from these models of the boundary layer thickness and of the velocity profile in the case of a periodic wave propagating over a fixed rough bottom do not agree very well with the experimental data when dealing with large roughness elements. In particular, the predicted boundary layer thickness δ, using the Grant and Madsen (1986) eddy viscosity model (hereafter referred to as the Grant-Madsen or the GM model), is two to three times smaller than the one obtained experimentally by Mathisen (1993). The purpose of this work is to try to improve the GM model by expressing the eddy viscosity differently. Indeed, the relation between the velocity and the shear stress is not well understood. The simplest way of getting around this problem involves the use of the eddy viscosity concept. With this, the relation between u and τ is defined, by analogy with the laminar case, as

$$\tau = \rho \nu_t \frac{\partial}{\partial z}(\tilde{u} - \tilde{u}_b). \tag{1.16}$$

Equation (1.2) takes then the form

$$\frac{\partial}{\partial t}(\tilde{u} - \tilde{u}_b) = \frac{\partial}{\partial z}\left\{\nu_t \frac{\partial}{\partial z}(\tilde{u} - \tilde{u}_b)\right\}. \tag{1.17}$$

and the problem becomes how to define the eddy viscosity, ν_t. The main difference between the models is, as we will see in next chapters, the way the eddy viscosity is expressed. This will lead to substantially different solutions.

1.3 Outline

A drag law interpretation of the flow resistance over a rippled bottom is presented in Chapter 2. An expression for the drag coefficient, C_D, in terms of the ripple dimensions and the energy dissipation is obtained, which, using Mathisen's (1993) experimental results for energy dissipation over artificial roughness, suggests a dependency of C_D on the ratio of the ripple height over the bottom excursion amplitude, η/A_b. This result is in qualitative agreement with Sarpkaya's analysis (Sarpkaya and Isaacson 1981) of the drag coefficient as a function of the Keulagan-Carpenter number.

From the C_D expression a dissipation rate similar to that of a laminar flow is obtained. Since the drag law approach is not specific to any type of flow, and since the laminar formulation is similar in nature to that of a turbulent flow with a constant eddy viscosity, the drag law results are also used in combination with other proposed eddy viscosity models.

In Chapter 3 the eddy viscosity is considered constant throughout the bottom boundary layer and an expression for it, in terms of flow and bottom parameters, is obtained. This expression is in turn compared to Sleath's (1991) constant eddy viscosity , and the similarities and differences are highlighted. The Constant eddy viscosity model, similar to the laminar model presented in Section 1.1, is applied with the linearized boundary layer equation to predict detailed velocity magnitude and phase profiles. These results are compared to the classical Grant-Madsen model's prediction and to measurements from Mathisen (1993) and Barrantes (1996). The classical Grant-Madsen model's inability to predict accurately the details of the velocity profile is shown graphically.

In Chapter 4 a new bottom boundary condition is included in the classical Grant-Madsen model formulation, and a Modified Grant-Madsen model is derived. This modification allows this linearly varying eddy viscosity model to be able to predict the velocity profile close to the bottom. The new model is then compared to the Constant eddy viscosity model, in terms of the details of the velocity profile, and

the Constant eddy viscosity model appears to give a better prediction of the velocity profile. Then, motivation to proceed with the development of a third eddy viscosity model is given.

In Chapter 5 a model which combines the two previous models is derived and another comparison of each model's velocity profile predictions is performed, showing that the Constant eddy viscosity model and the Combined model give similar results. Additional work is done in Chapter 6 to analyze the performance of the Constant eddy viscosity model and the Combined model in predicting the energy dissipation due to the flow bottom interaction. This is done by comparing the values of the energy dissipation factor obtained theoretically from each model with direct measurements performed by several authors in wave tunnels and wave flumes over fixed and movable beds. Finally, the conclusions are presented in Chapter 7.

Chapter 2

Drag Model

When large roughness elements are present, a simple way of looking at the flow-bottom interaction is in terms of the force acting on the roughness elements or, equivalently, the resistance or retarding force experienced by the flow.

The fluid forces acting on the roughness elements are of two kinds: namely drag forces and pressure forces resulting from pressure gradients in the fluid. On one hand, pressure forces can be evaluated on the basis of inviscid flow theory. On the other hand, drag forces occur as form drag, which is translated in flow separation and eddy formation, and as skin friction, which, in the case of large roughness elements, are produced mainly by the roughness of the bedform surface and not by the bedform itself.

The drag forces are not easy to evaluate, mainly because they are related to the generated turbulence. This difficulty is expressed mathematically in terms of the drag coefficient, which depends on the flow and the shape of the submerged bodies.

2.1 A Simple Drag Coefficient Relationship

In nature, by large roughness elements we usually refer to sand ripples. In the laboratory, those ripples can be modeled as two-dimensional roughness elements perpen-

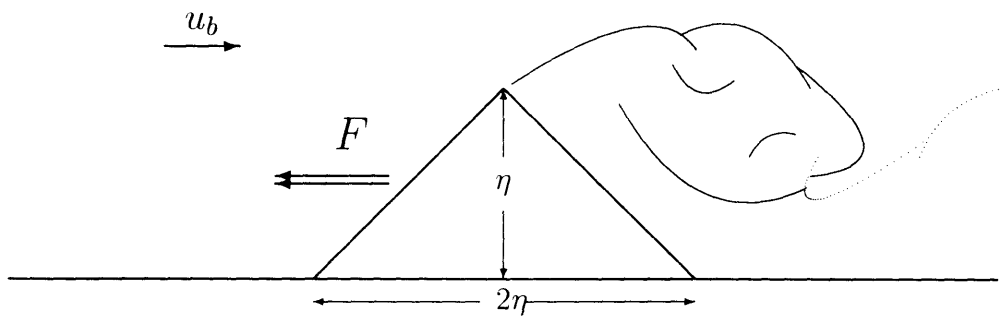

Figure 2-1: Separation and eddy formation downstream a standard artificial ripple.

dicular to the flow direction, as shown in Figure 2-1.

The total force per unit length experienced by the bedform due to the flow is

$$F = \frac{1}{2}\rho C_D \eta |\tilde{u}_b| \tilde{u}_b + \rho(1 + C_a)\forall \frac{d\tilde{u}_b}{dt}, \tag{2.1}$$

where ρ is the water density, η is the ripple height, C_a is the added mass coefficient, and $\forall$ is the volume of the bedform per unit width.

This equation is equivalent to the Morison equation (see, *e.g.*, Sarpkaya and Isaacson,1981,), which expresses the force acting on a section of a pile due to wave motion. The first term is the drag force and the second term is the inertia. With $\tilde{u}_b = u_b \cos \omega t$, Equation (2.1) can be written as

$$F = \frac{1}{2}\rho C_D \eta u_b^2 |\cos \omega t| \cos \omega t - \rho C_m \forall u_b \omega \sin \omega t, \tag{2.2}$$

where $C_m = 1 + C_a$ is the inertia coefficient.

It can be seen that there is a phase shift ϕ between F_{max} and $\tilde{u}_{b,max}$, i.e., the maximum velocity at a given location does not occur at the same time as the maximum force is exerted on the bottom. From Equation (2.2), this phase angle is $\phi = \arcsin((C_m \forall \omega)/(C_D \eta u_b))$. In Figure 2-2 F and u_b are plotted as functions of ωt for typical experimental values of the different parameters involved. The values used correspond to Mathisen's (1993) Experiment "a" : $C_D = 2.3$; $u_b = 17\ cm.s^{-1}$; $\omega = 2.8\ rad.s^{-1}$; and $\forall = \eta^2 = 2.25\ cm^2$. The inertia coefficient was obtained from

Newman (1977, Table 4.3), where the added mass coefficient for a square with side $\sqrt{2}\,\eta$ is $C_{a,square} = 2.377$. Therefore, for a ripple, i.e., half a square, we can take $C_{a,ripple} = C_{a,square}/2 \simeq 1.19$. With these values the phase shift is $\phi = 13.6°$. It is important to notice that, as well as in the laminar flow model, the phase shift feature is present, but here it is a function of flow and bottom characteristics.

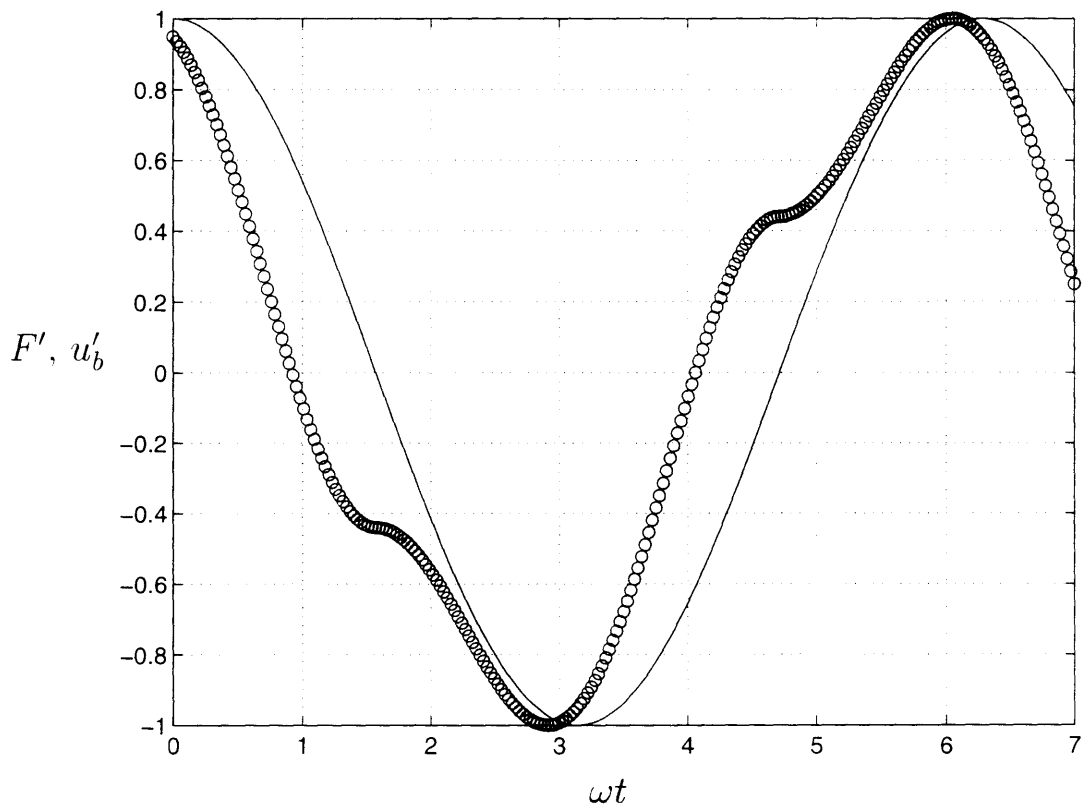

Figure 2-2: Total force experienced by the bedform, F, and bottom velocity $\tilde{u}_b$ as a function of time. Both functions have been normalized as $F' = F/F_{max}$ (*circles*) and $\tilde{u}_b' = \tilde{u}_b/u_b$ (*solid line*).

The bottom shear stress can be expressed as the ratio of the force exerted on the bedform over the length of the bedform:

$$\tau_b = \frac{F}{\lambda}. \tag{2.3}$$

With this and Equation (2.2), the energy dissipation, as defined in Chapter 1 as

$E_d = \overline{\tau_b \tilde{u}_b}$, can be written as

$$E_d = \frac{1}{2}\rho C_D \frac{\eta}{\lambda} u_b^3 \overline{|\cos\omega t| \cos^2 \omega t} - \rho C_m \forall u_b^2 \frac{\omega}{\lambda} \overline{\sin\omega t \cos\omega t} = \frac{2}{3\pi}\rho C_D \frac{\eta}{\lambda} u_b^3. \tag{2.4}$$

Another way of defining the energy dissipation is in terms of an energy dissipation factor. Indeed, we can assume the bottom shear stress to be simple periodic and write it in terms of a friction factor as

$$\tau_b = \frac{1}{2}\rho f_w u_b^2 \cos(\omega t + \varphi_t), \tag{2.5}$$

where f_w is the friction factor and φ_t is the phase angle between the bottom shear stress and the free stream wave orbital velocity. This leads to an energy dissipation

$$E_d = \frac{1}{4}\rho f_e u_b^3, \tag{2.6}$$

where $f_e = f_w \cos\varphi_t$ is the energy dissipation factor.

It is important to point out here that, for large bottom roughness, this phase difference is not negligible.

Finally, from Equations (2.4) and (2.6) we get:

$$C_D = \frac{3\pi}{8}\frac{\lambda}{\eta} f_e. \tag{2.7}$$

This equation shows a functional form of the drag coefficient in terms of the ripple dimensions and the energy dissipation inside the boundary layer. The drag coefficient can then be evaluated with the knowledge of the ripple dimensions and the energy dissipation factor, which in turn is obtained from wave attenuation measurements.

2.2 Experimental Data

The data used to get the drag coefficient relationships comes from the experimental measurements obtained by Paul Mathisen in his Ph. D. dissertation (1993). The experiments were performed in a wave flume, where pure monochromatic waves were run over 1.5 cm high bars perpendicular to the flow and with a spacing of 20 cm between bars (experiments m, n, and o) and 10 cm (all the others). Table 2.1 gives the data summarizing the characteristics of each experiment. The details of the experimental setup can be found in Mathisen (1993).

Table 2.1: Artificial Bedform Data from Mathisen (1993)

Experiment	T (s)	λ (cm)	η (cm)	A_b (cm)	f_e
a	2.24	10	1.5	6.09	0.297
b	2.63	10	1.5	7.9	0.224
c	2.89	10	1.5	8.84	0.183
d	2.24	10	1.5	4.2	0.362
e	2.63	10	1.5	5.72	0.291
f	2.89	10	1.5	6.21	0.265
m	2.24	20	1.5	5.95	0.152
n	2.63	20	1.5	7.97	0.129
o	2.89	20	1.5	9.15	0.099

From this data and using Equation (2.7), the drag coefficient was obtained for each experiment. After looking, by trial and error , for the dependency of C_D on different parameters of the flow and the bottom roughness, as η/λ and η/A_b, a relatively strong dependency of C_D on η/A_b was found. This dependency is shown in Table 2.2 and Figure 2-3.

Based on the best linear fit, forcing the intercept to be zero, as seen in Figure 2-3, the relation was obtained

$$C_D = \frac{1}{0.1114}\frac{\eta}{A_b} \approx 9\frac{\eta}{A_b} \stackrel{\text{def}}{=} C_{D_0}\frac{\eta}{A_b}, \tag{2.8}$$

Table 2.2: Drag Coefficient and wave parameters for each experiment.

Experiment	C_D	η/A_b
a	2.333	0.246
b	1.759	0.190
c	1.437	0.170
d	2.843	0.357
e	2.286	0.262
f	2.081	0.242
m	2.388	0.252
n	2.026	0.188
o	1.555	0.164

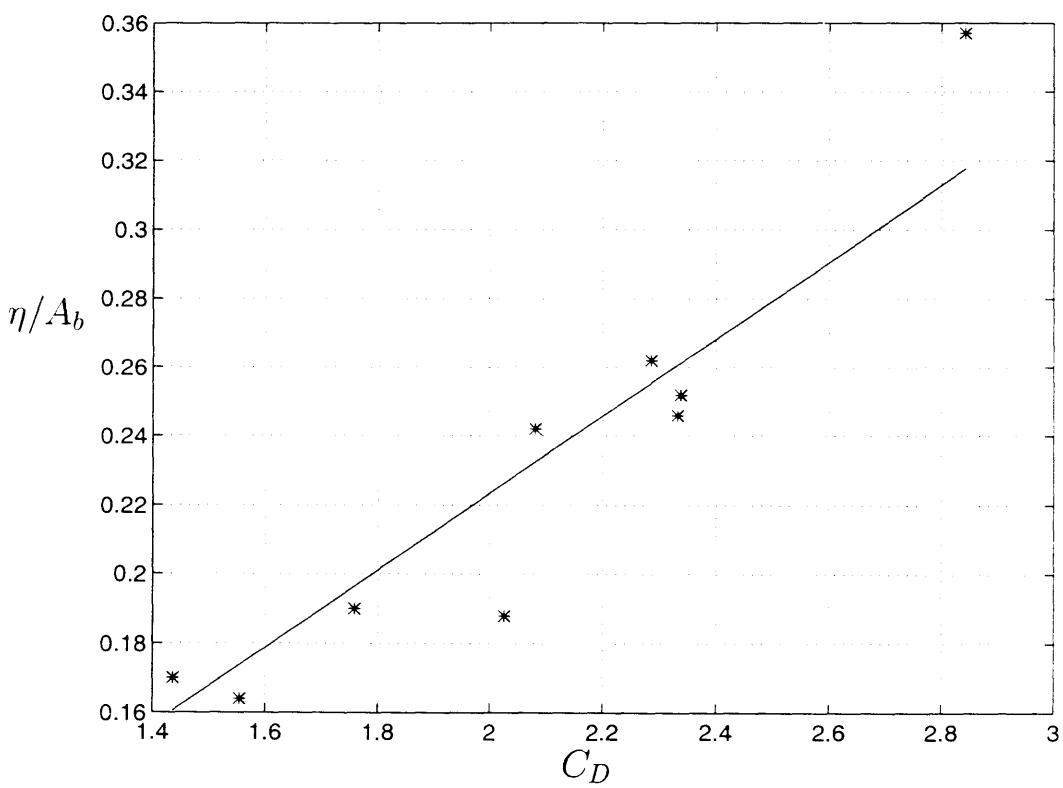

Figure 2-3: Ratio of the ripple height over the bottom excursion amplitude, η/A_b, as a function of the drag coefficient, C_D. Experimental values (*circles*) and linear fitting (*solid line*). The coefficient of determination is $r^2 = 0.87$.

This relation, Equation (2.8), has a coefficient of determination $r^2 = 0.87$ indicating that 87 % of the original uncertainty has been explained by the linear model. The standard error of the estimate (see, *e.g.*, Devore, 1991) is $S_{y/x} = 0.0233$, which is the standard difference between the experimental and the fitted η/A_b. It can further be said with an 80 % confidence level, that the slope C_{D_0} lies between 7.19 and 10.62.

Another way of measuring the strength of the relation between C_D and η/A_b is to analyze its variability. Assuming that the errors of the estimate follow a normal distribution, values of η/A_b can be simulated and new fittings can be obtained. Indeed, with the knowledge of $S_{y/x}$, an error can be simulated as a random number r_i picked from a normal distribution with zero mean and standard deviation $S_{y/x}$. This error can then be added to the fitted value of η/A_b to get a simulated η/A_b as $(\eta/A_b)' = (C_D/C_{D_0}) + r_i$. Repeating this procedure for each experiment a simulated slope of the fitting and the corresponding coefficient of determination are obtained. In Figure 2-4 are plotted 100 simulations of the slope.

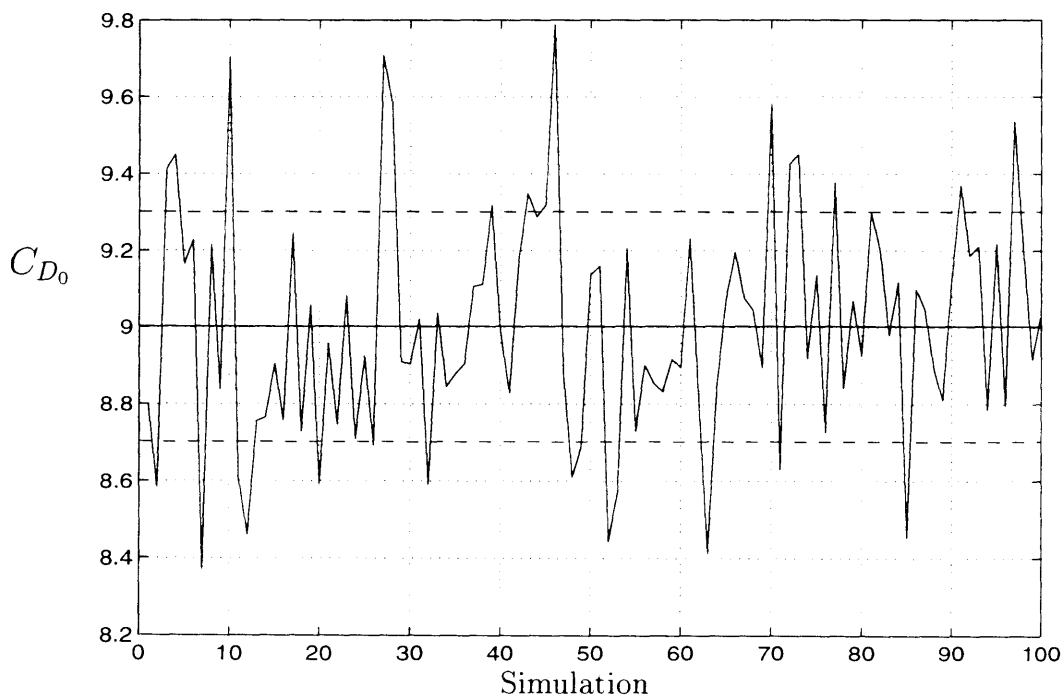

Figure 2-4: Slope C_{D_0} for 100 sets of simulated η/A_b. The three horizontal lines are the mean slope (*solid line*) and the 66% confidence interval (*dashed lines*).

Also show in the figure are the mean simulated slope, which is $\overline{C_{D_0}} = 9.00$ and the 66% confidence interval, which goes from 8.70 to 9.30. The mean coefficient of determination for the simulations is $\overline{r^2} = 0.81$ and the standard deviation is 0.11, which shows a weaker average fitting, compared to the fitting obtained with the real data. However, the overall observation is that the C_D dependency on η/A_b is real and can be used for further analysis of the flow-bottom interaction.

2.3 Analogy with the Keulegan-Carpenter Number

The parameter η/A_b used so far is the ripple height relative to the amplitude of the fluid motion. Sarpkaya and Isaacson (1981) studied the dependency of the drag coefficient on this parameter, or some equivalent relation, as was originally done by Keulegan and Carpenter and later by several other authors. Indeed, Keulegan and Carpenter established what is now called the Keulegan-Carpenter number from experimental results of oscillatory flow around a cylinder, relating the fluid maximum orbital velocity u_b, the period of oscillation T, and the cylinder diameter D, as

$$K = \frac{u_b T}{D}, \tag{2.9}$$

or, in terms of the excursion amplitude,

$$K = 2\pi \frac{A_b}{D}. \tag{2.10}$$

The analogy between this problem and waves running over a movable bed has to be made carefully. Indeed, for a movable bed the water is not flowing around the ripple as in the case of the cylinder, since the ripples are on the bottom of the channel. For this reason, it would not be accurate to replace D by the ripple height η. However, by using the concept of images, which is sketched in Figure 2-5 and is

used to account for the existence of a solid boundary, it can be seen that a better measure of the obstacle would be 2η.

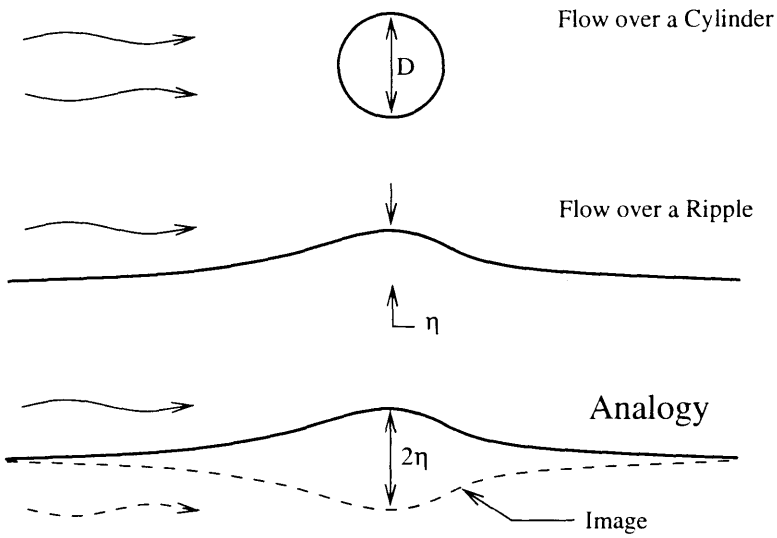

Figure 2-5: Analogy between flow over a cylinder and flow over a ripple.

Therefore, replacing the cylinder diameter by two times the ripple height in Equation (2.10), an equivalent Keulegan-Carpenter number K for waves over a rippled bottom would be

$$K = \pi \frac{A_b}{\eta}. \tag{2.11}$$

This K is, by a factor of π, the inverse of the parameter that was used to obtain a general expression for the drag coefficient, Equation (2.8), which, combined with Equation (2.11) gives an expression relating the drag coefficient and the Keulegan-Carpenter number

$$C_D \cong \frac{28}{K}. \tag{2.12}$$

In Figure 2-6 are plotted the results obtained by Sarpkaya in 1976 (see Sarpkaya et al., 1981, Fig. 3-15), for flow around a cylinder and our results, copied from Figure 2-3.

It can be seen that, even if the Reynolds number in Mathisen's experiments ($3.5 \cdot$

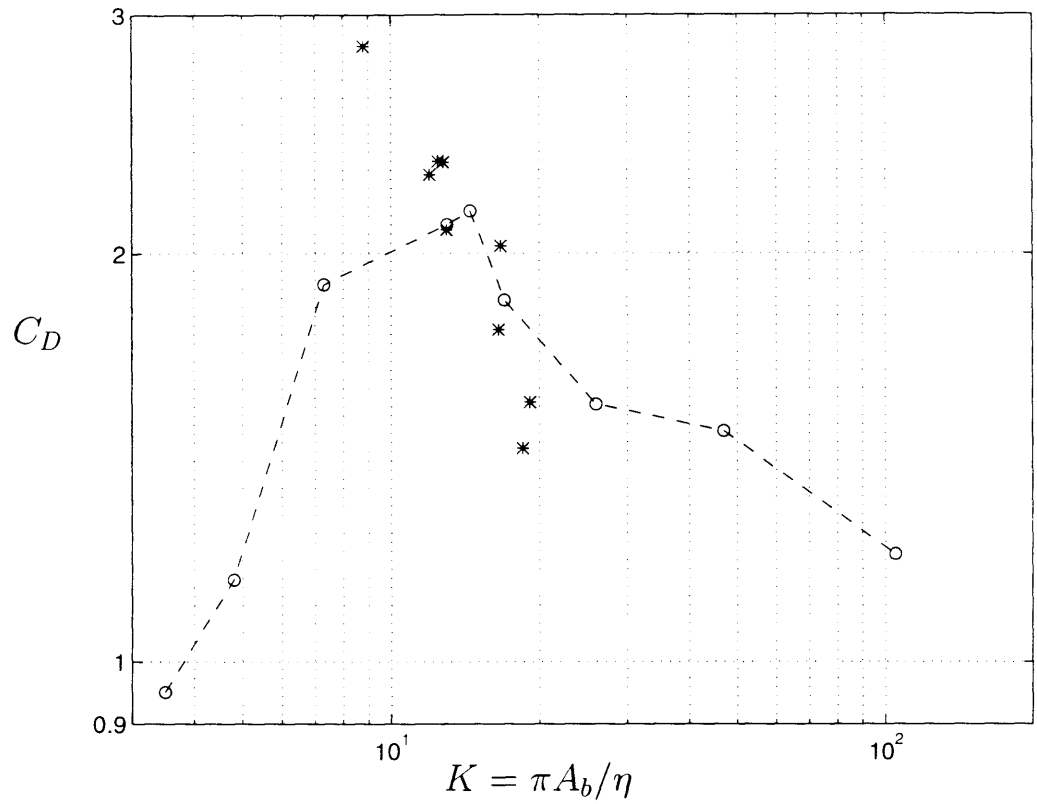

Figure 2-6: Drag coefficient as a function of the Keulegan-Carpenter number. Sarpkaya's experimental results (*circles and dashed line*); Mathisen's (1993) experimental results (*stars*).

$10^3 - 6.0 \cdot 10^3$) is smaller than the one in Sarpkaya's experiments, which is 10^4, the trend is similar for the same range of K, i.e., C_D decreases as K increases. Additionally, the fact that there is this agreement between experiments made with completely different conditions (cylinders and fixed roughness) suggests that the dependency of C_D on η/A_b obtained from these experiments is reasonable. It is important to say that the validity of Equation (2.8) is limited to the range of η/A_b from which it was obtained. Indeed, for $A_b \to \infty$, i.e. steady flow, C_D should tend to a constant non-zero value and not to zero as suggested by Equation (2.8). Also, if A_b tends to zero C_D should also tend to zero, which is the opposite to what Equation (2.8) suggests.

The relation between C_D and η/A_b can now be used to obtain a new expression

for the energy dissipation. From Equations (2.4) and (2.8) we get:

$$E_d = \frac{2}{3\pi} C_{D_0} \rho \omega \frac{\eta^2}{\lambda} u_b^2, \tag{2.13}$$

which, in terms of its functional dependency on the velocity squared, is similar to the energy dissipation obtained from the laminar model, Equation (1.14).

Chapter 3

Constant Eddy Viscosity Model

The drag model suggests, through its prediction of the energy dissipation rate similar to that of a laminar model, that a Constant eddy viscosity model may be used successfully to describe the flow within the wave bottom boundary layer. In fact, the Constant eddy viscosity model is completely analogous to the laminar model presented in Chapter 1. The only difference is that the kinematic viscosity ν is replaced by the constant eddy viscosity ν_t. Therefore the solutions are the same and, in particular, the energy dissipation becomes

$$E_d = \frac{\sqrt{2}}{4}\rho\sqrt{\nu_t\omega}\, u_b^2. \tag{3.1}$$

3.1 Experimental Data

On one hand Equation (3.1) can be combined with Equation (2.13) to get an expression for the eddy viscosity in terms of the period and the roughness dimensions as

$$\nu_t = \frac{64}{9\pi}C_{D_0}^2\frac{\eta^4}{\lambda^2 T} \equiv \nu_{t_0}\frac{\eta^4}{\lambda^2 T} \tag{3.2}$$

where ν_{t_0} is another constant.

This shows that the drag law approach can be translated to a constant eddy

viscosity approach, i.e., the C_D dependency on η/A_b is equivalent to a ν_t dependency on $\eta^4/(\lambda^2 T)$. For $C_{D_0} = 9$, as obtained in Section 2.2, we get $\nu_{t_0} = 183.3$.

On the other hand, Equation (3.1) can be combined with Equation (2.6) in order to relate ν_t with f_e as

$$\nu_t = \frac{1}{4\pi} T f_e^2 u_b^2. \tag{3.3}$$

With this and the knowledge of f_e, u_b and T (from Table 2.1) an estimate of the eddy viscosity can be obtained and a fit can be performed for ν_t as a function of $\eta^4/(\lambda^2 T)$, as seen in Figure 3-1, where $\nu_{t_0} = 178.8$.

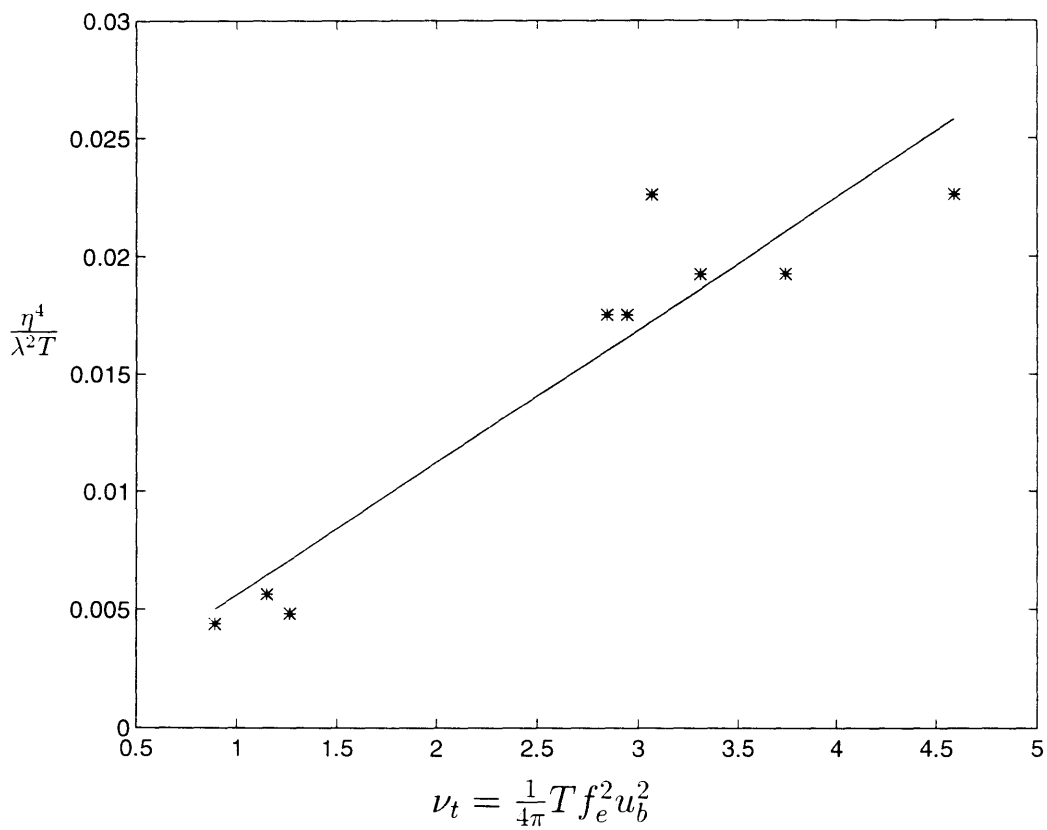

Figure 3-1: Eddy Viscosity ν_t as a function of $\eta^4/(\lambda^2 T)$. Both quantities are in $(cm^2.s^{-1})$. Experimental values obtained from Equation (3.3)(*crosses*) and linear fitting (*solid line*). The coefficient of determination is $r^2 = 0.91$.

Given the statistical nature of the fitting procedure, the difference in ν_{t_0} using Equation 3.2 and using the fitting shown in Figure 3-1 is irrelevant and the constant

eddy viscosity can be expressed as

$$\nu_t \cong 180\frac{\eta^4}{\lambda^2 T}. \tag{3.4}$$

3.2 Comparison with Sleath's Constant Eddy Viscosity Model

As shown in Sleath (1991), another way to express the eddy viscosity is in terms of parameters that characterize the turbulence itself. Indeed, the eddy viscosity can be expressed as

$$\nu_t = v'\ell, \tag{3.5}$$

where v' is the vertical velocity fluctuation and ℓ is the mixing length. In the vicinity of the bed, he considers the mixing length to be proportional to the height above the bed, i.e.,

$$\ell \propto z. \tag{3.6}$$

Based on measurements from experiments performed in 1987 (see Sleath, 1987) in an oscillatory flow water tunnel with flat beds of sand, gravel and pebbles, Sleath found that the vertical velocity fluctuation is inversely proportional to the height above the bed and showed that the eddy viscosity is independent of the height above the bottom.

To obtain this result he first makes the analogy between the bottom generated turbulence and the turbulence generated by a regular grid oscillating in still water. In both cases the turbulence is mainly due to the formation and release of vortices behind the roughness elements (bottom roughness or grid) at the end of each half cycle of the oscillatory motion. These vortices interact with each other and with previous vortices to produce a pattern of turbulent eddies which decay with height above the bed (or grid). He uses then an expression from E and Hopfinger (1986) for

the fluctuation in velocity perpendicular to the direction of oscillation of a regular grid with mesh size M, and translates M directly into the length of the roughness elements to show that v' can be written as

$$v' = 0.16\frac{A_b^{3/2}k_N^{1/2}}{zT}, \tag{3.7}$$

where A_b is the amplitude of the oscillation, k_N is the roughness length, z is the height above the bed and T is the period of oscillation. Letting A be the constant of proportionality between ℓ and Z and using Equations (3.6) and (3.7), Equation (3.5) becomes

$$\nu_t = 0.16A\frac{A_b^{3/2}k_N^{1/2}}{T} \equiv A'\frac{A_b^{3/2}k_N^{1/2}}{T}, \tag{3.8}$$

The constant A usually corresponds to the von Kármán constant, i.e., it has a value of 0.4, but Sleath found experimentally that for the oscillatory component of the velocity the constant was between 0.1 and 0.2. This equation shows a similar feature to Equation (3.4), which is an eddy viscosity independent of the height above the bottom, and inversely proportional to the wave period.

Now, considering the roughness length for a rippled bed to be proportional to the ripple height η, Sleath's (1985) experiments for oscillatory flow over an artificial bed consisting of sinusoidal ripples can be used, in addition to Mathisen's (1993) data , to test Sleath's model and the Constant eddy viscosity model presented here. Mathisen's experiments specifications are shown in Table 2.1.

Sleath's experiments over sinusoidal ripples were performed with only one ripple dimension: $\lambda = 7.3$ cm and crest-to-trough height 1.7 cm. This height is assumed here to be equivalent to Mathisen's η. Both, the unique ripple dimension and the last assumption, can be of some concern and have to be taken into account, as will be shown later in this Section.

For the purpose of the comparison, we must express both models with equivalent

equations. Thus, Equation (3.4) may be written as

$$\nu_t = \left[\frac{180}{\alpha^{1/2}}\left(\frac{\eta}{A_b}\right)^{3/2}\left(\frac{\eta}{\lambda}\right)^2\right]\frac{A_b^{3/2}k_N^{1/2}}{T} \equiv B\frac{A_b^{3/2}k_N^{1/2}}{T}, \tag{3.9}$$

where α is the proportionality constant between k_N and η.

Given typical values from Mathisen's data for η/λ and η/A_b, the term inside the brackets in the last expression can eventually be considered as a constant, namely B. Equation (3.9) acquires then the same form as Equation (3.8), and the constant B can be compared to the constant A'. Assuming $\alpha = 4$ as suggested by Grant and Madsen (1982) for steep ripples, and using Mathisen's artificial bedform experiments, Table 2.1, the value of B lies between 0.14 and 0.43 for the experiments with $\lambda = 10$ cm, and in the range 0.03 to 0.06 for the experiments with $\lambda = 20$ cm. This shows that the Constant eddy viscosity model presented here and Sleath's model (Sleath 1991) differ in the sense that the constant B obtained from Mathisen's experiments is, in most of the cases, significantly larger than the value of A' obtained by Sleath, which is at most equal to 0.032.

Conversely, Equation (3.8) could be transformed to become similar to Equation (3.4) and another comparison could be made. However, the constant in that equation would involve Sleath's constant A and the constant of proportionality α and, at present, we do not have the tools to determine accurately the value of those constants for sinusoidal ripples. Therefore, by assigning, to some degree arbitrarily, the right values to those constants we could make the models look equivalent, but this result would be artificial.

Additionally, for the models to be comparable, Mathisen's data should show a dependency of ν_t on $A_b^{3/2}/T$, while Sleath's data should show a dependency of ν_t on $\eta^4/(\lambda^2 T)$. However, this is not the case, as shown in Figure 3-2.

Indeed, when testing Sleath's model with Mathisen's data and the Constant eddy viscosity model presented here with Sleath's data, the fitting in both cases is very

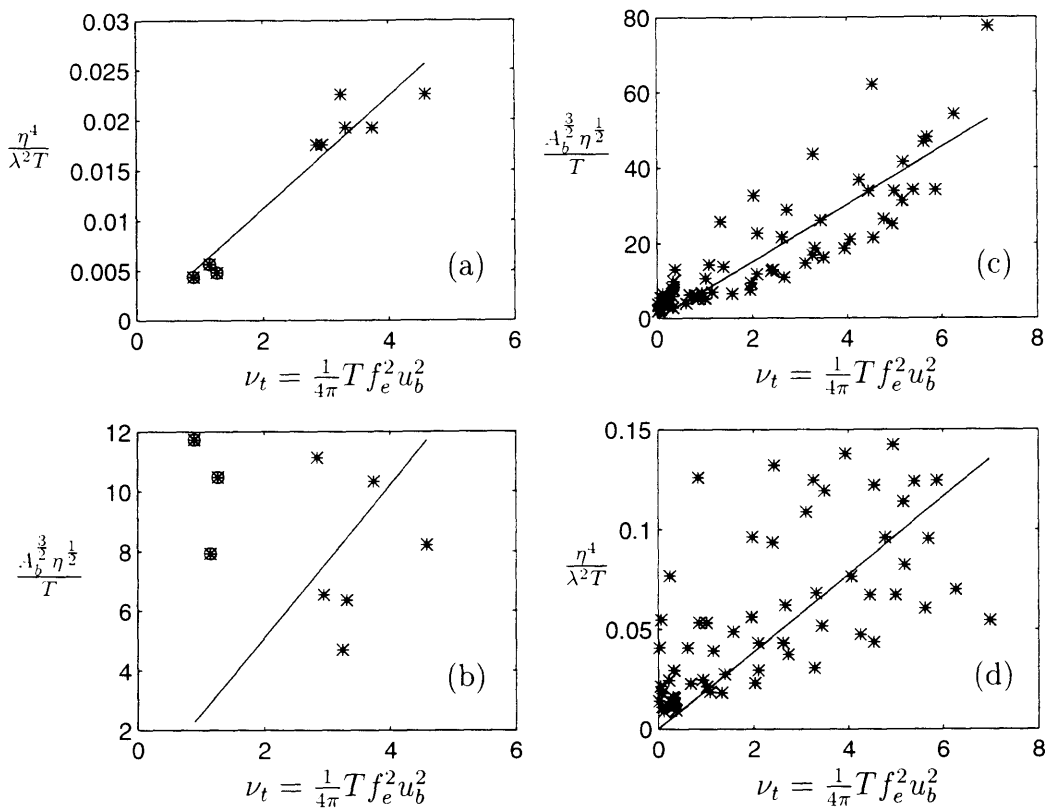

Figure 3-2: Comparison between Sleath's (1991) model and the Constant eddy viscosity model presented here using data from Sleath (1985) and Mathisen (1993). **(a)** ν_t as a function of $\eta^4/(\lambda^2 T)$ using Mathisen's data; $r^2 = 0.91$. **(b)** ν_t as a function of $(A_b^{3/2}\eta^{1/2})/T$ using Mathisen's data; $r^2 = 0$. **(c)** ν_t as a function of $(A_b^{3/2}\eta^{1/2})/T$ using Sleath's data; $r^2 = 0.73$. **(d)** ν_t as a function of $\eta^4/(\lambda^2 T)$ using Sleath's data; $r^2 = 0.19$. Experimental values (*crosses*) and linear fittings (*solid lines*). The circled data points in (a) and (b) correspond to the experiments with $\lambda = 20cm$. All the axis have the unit of $cm^2.s^{-1}$.

poor, as seen in Plots (b) and (d), where the coefficients of determination are $r^2 = 0$ and $r^2 = 0.19$, respectively.

For Plot (d), where Sleath's data is used with the Constant eddy viscosity model presented here, the slope is $\nu_{t_0} = 51.6$. Even if the correlation coefficient for this fit is small, this value of ν_{t_0}, which is more than three times smaller than the ν_{t_0} obtained with Mathisen's data, is in good agreement with the intuitive idea that the turbulence generated by a sinusoidal bottom is smaller than the turbulence generated by steep ripples.

Moreover, it is reasonable to say that the translation of Sleath's sinusoidal ripple crest-to-trough height into η is in some way an overestimation of the ripple height. Indeed, given the smooth nature of the sinusoid, the trough and crests concepts in a sinusoidal bed configuration are not as sharply defined as in Mathisen's experiments bottom configuration. A sharp ripple with a height equal to the crest-to-trough height of a sinusoidal ripple would exert a stronger resistance to the flow than the sinusoidal ripple itself. So, a better interpretation of the ripple height in a sinusoidal ripple would be a fraction of the crest-to-trough height. This would produce an increase in the slope ν_{t_0}, which in turn would mean a better agreement with the results obtained with Mathisen's data. However, by scaling the value of η in Sleath's data, the coefficient of determination for the fit in plot (d) would drop dramatically, meaning that the dependency of ν_t on $\eta^4/(\lambda^2 T)$ would be lost.

Besides, a good fitting in Plots (b) and (d) would mean that the two models are to some degree equivalent, which in turn would mean that there is a linear relation between $(A_b^{3/2}\eta^{1/2})/T$ and $\eta^4/(\lambda^2 T)$, or simply between $A_b^{3/2}$ and $\eta^{7/2}/\lambda^2$. It is clear that this dependency is unlikely to happen in experiments where the bottom is fixed. Therefore, the study of this dependency should be made with experiments of oscillatory flow over movable bed.

For comparison with Plots (b) and (d), the fit of Mathisen's data using our Constant eddy viscosity model and the fit of Sleath's data (Sleath 1985) using his model are plotted in (a) and (c), respectively.

The slope for Plot (c) is 0.132, which, assuming again $k_N = 4\eta$, would give a new version of Equation (3.8) for two-dimensional roughness elements with the proportionality constant equal to 0.066, instead of A' (which is between 0.016 and 0.032 for A between 0.1 and 0.2). This suggest, first that the idea of making $A = \kappa = 0.4$ when dealing with sinusoidal ripples, which would mean $A' = 0.064$, should be revisited, and second that more work has to be done in order to analyze whether the value of 4η for k_N or the value of 0.1 or 0.2 for Sleath's constant A are valid and

applicable to all type of bottom bedforms.

As seen above, the two models share the feature that they are both based on an eddy viscosity which is constant with respect to the height above the bottom. However, they are not compatible in terms of the functional form of the eddy viscosity.

3.3 Velocity Profile Prediction

Finally, we look to the Constant eddy viscosity model and the classical GM model predictions of the velocity profile measurements from Mathisen (1993). The GM model assumes $\nu_t = \kappa u_* z$ for the complete range $0 \leq z < \infty$ and the bottom boundary condition is $u = 0$ for $z = z_0$. A complete derivation of the model for waves and currents can be seen in Grant and Madsen (1986). The Constant eddy viscosity model uses Equation (1.8), replacing ν by ν_t from Equation (3.4). The velocity measurements were made over the trough and over the crest of the ripples and, as seen in Figure 3-3, the velocity amplitude over the crest is significantly larger than the velocity over the trough, for $z \leq 4$ cm, where the so-called overshoot takes place. The increase in velocity over the crest is mainly due to the reduction in cross-sectional area, as predicted by potential flow theory. Since this difference between the trough and the crest velocity amplitudes is not taken into account by any of the models, the crest measurements are shown only for completeness. Therefore, the measurements that have to be compared with the model predictions are the trough measurements, which are more representative of the average velocity profile, given the dimensions of the artificial ripples and the separation between them.

In a first inspection, Figure 3-3 shows that the Constant eddy viscosity model gives a good prediction of the measured velocity amplitude over the trough of the ripples and a relatively better prediction of the measured velocity phase, than does the Grant-Madsen model prediction.

The figure also shows that the GM model is not applicable when dealing with

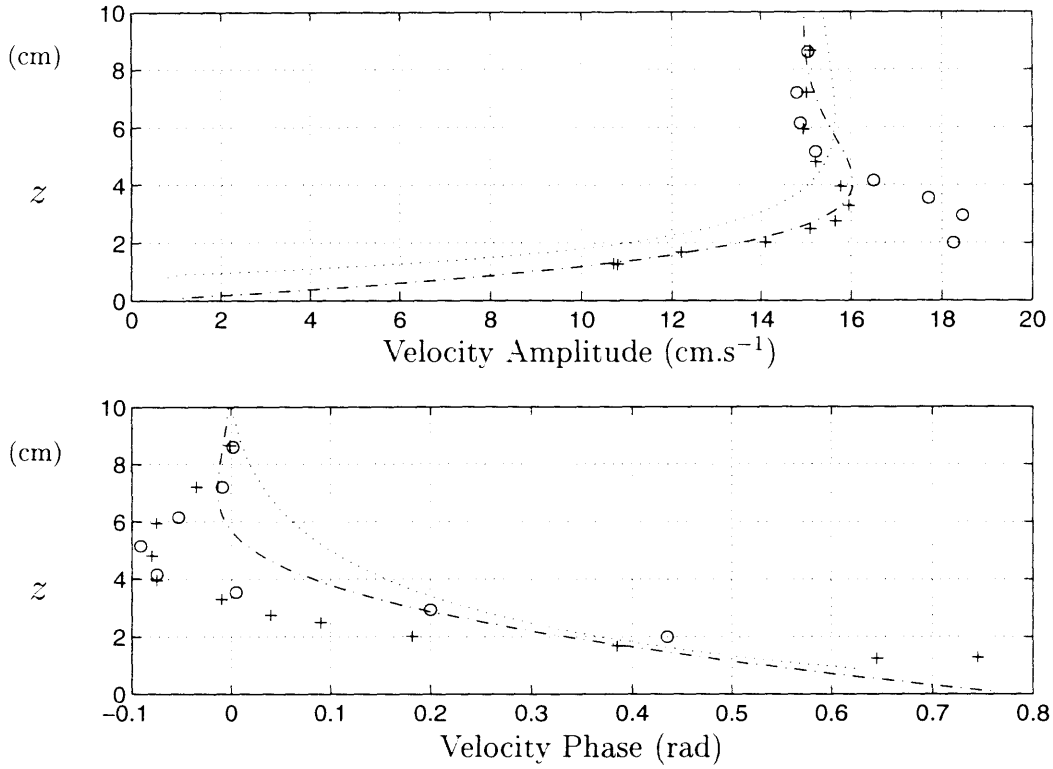

Figure 3-3: Velocity profiles obtained from 1) the classical Grant-Madsen eddy viscosity model (*dotted line*), 2) the Constant eddy viscosity model presented here (*dash-dotted line*), and 3) Mathisen's Experiment "a" measurements above the trough of the ripples (*pluses*) and above the crest of the ripples (*circles*). The input parameters for the models corresponding to experiment "a" are shown in Table 2.1. The GM model needs the additional information of the bottom roughness magnitude, which is shown in Table 4.1.

large roughness elements. Indeed, according to the boundary condition specified in that model, the solution is only valid for $z \geq z_0$. The problem is that for ripples $z_0 = k_n/30$ becomes large enough to produce a non-negligible gap in the velocity profile for $0 \leq z \leq z_0$. This suggests that an improvement in terms of the velocity profile prediction close to the bottom should be tried by studying an equivalent model valid for this range.

Chapter 4

Modified Grant-Madsen Model

As shown in Section 3.3 and Figure 3-3, the classical Grant-Madsen model's prediction of the velocity profiles becomes inaccurate in the near vicinity of the bottom. In fact, it cannot predict the velocity for $0 \leq z < z_0$, which is an important part of the bottom boundary layer when z_0 is large, i.e., when the bottom consists of large roughness elements.

In this Chapter we will show in the first section that a modified model, which is applicable for $0 \leq z < \infty$, can be easily obtained. Then, a more strict comparison with the Constant eddy viscosity model is made, in terms of the detailed velocity profile within the bottom boundary layer.

4.1 Theoretical Formulation

4.1.1 Velocity Solution

As in the classical GM model, the eddy viscosity is not independent of the height above the bottom anymore. Here, the eddy viscosity will be expressed as

$$\nu_t = \kappa u_*(z + z_0), \tag{4.1}$$

instead of $\nu_t = \kappa u_* z$. In that equation, κ is the von Kármán constant, z is the height above the bed, and z_0, which is proportional to the bottom roughness, is defined as $z_0 = k_N/30$. Additionally, u_* is the shear velocity and is defined as

$$u_* = \sqrt{\frac{\tau_{b,max}}{\rho}} = u_b\sqrt{\frac{f_w}{2}}, \tag{4.2}$$

With Equation (4.1), the equation of motion for turbulent flow, Equation (1.17), can be rewritten as

$$\frac{\partial}{\partial t}(\tilde{u}_d) = \frac{\partial}{\partial z}\left\{\kappa u_*(z+z_0)\frac{\partial \tilde{u}_d}{\partial z}\right\}, \tag{4.3}$$

where $\tilde{u}_d$ is the deficit velocity defined as

$$\tilde{u}_d = \tilde{u} - \tilde{u}_b. \tag{4.4}$$

Expanding and using the definition of the tilde notation, Equation (1.7), Equation (4.3) simplifies to

$$iu_d = \frac{\partial}{\partial z}\left\{\frac{\kappa u_*}{\omega}(z+z_0)\frac{\partial u_d}{\partial z}\right\}. \tag{4.5}$$

This equation can be further simplified by scaling the vertical coordinate by the boundary layer scale l as

$$\xi = \frac{z+z_0}{l}, \tag{4.6}$$

instead of $\xi = z/l$, as in the classical GM model, where

$$l = \frac{\kappa u_*}{\omega}. \tag{4.7}$$

Then Equation (4.5) becomes

$$iu_d = \frac{\partial}{\partial \xi}\left(\xi\frac{\partial u_d}{\partial \xi}\right), \tag{4.8}$$

which is a Bessel-type equation that has a general solution in terms of Kelvin func-

tions. With the boundary conditions

$$u_d \to 0 \; as \; \xi \to \infty, \; and \; u_d = -u_b \; at \; \xi = \xi_0 = z_0/l, \tag{4.9}$$

the solution of Equation (4.8) is

$$u_d = -u_b \frac{\mathrm{Ker}\,(2\sqrt{\xi}) + \mathrm{iKei}\,(2\sqrt{\xi})}{\mathrm{Ker}\,(2\sqrt{\xi_0}) + \mathrm{iKei}\,(2\sqrt{\xi_0})}, \tag{4.10}$$

where Ker and Kei are Kelvin functions of zeroth order, which can be evaluated with polynomial approximations from Abramowitz and Stegun (1972, page 384). This solution. is analogous to the original Grant-Madsen solution. The only difference is the definition of ξ, which makes the expression valid for the range $0 \leq z < \infty$ and gives rise to a no-slip condition at $z = 0$, instead of at $z = z_0$.

4.1.2 Closure

In Equation (4.10) the bottom roughness and the friction factor, involved in ξ, are still unknown. To close the problem, the definition of the maximum bottom shear stress is used to write

$$\frac{\tau_{b,max}}{\rho} = u_*^2 = \nu_t \left.\frac{\partial u}{\partial z}\right|_{z=0} = \frac{\nu_t}{l} \left.\frac{\partial u}{\partial \xi}\right|_{\xi=\xi_0}, \tag{4.11}$$

which, using the definition of the eddy viscosity, Equation (4.1), and the definition of the deficit velocity, Equation (4.4), can be written as

$$\frac{\tau_{b,max}}{\rho} = u_*^2 = \frac{\kappa u_*(z+z_0)}{l} \left.\frac{\partial u}{\partial \xi}\right|_{\xi=\xi_0}. \tag{4.12}$$

Substituting the expression for the deficit velocity, Equation (4.10), into this last equation we get

$$u_* = \kappa\sqrt{\xi_0} u_b \left|\mathbf{F}_{Mod}(\xi_0)\right|, \tag{4.13}$$

where

$$\mathbf{F}_{Mod}(\xi_0) = \frac{-\mathrm{Ker}'\left(2\sqrt{\xi_0}\right) - \mathrm{iKei}'\left(2\sqrt{\xi_0}\right)}{\mathrm{Ker}\left(2\sqrt{\xi_0}\right) + \mathrm{iKei}\left(2\sqrt{\xi_0}\right)}. \tag{4.14}$$

The phase angle between the shear stress and the near bottom velocity is given by

$$\varphi_t = \arctan\left(\frac{\Im m\ \left[\mathbf{F}_{Mod}(\xi_0)\right]}{\Re e\ \left[\mathbf{F}_{Mod}(\xi_0)\right]}\right). \tag{4.15}$$

In addition, from Equations (4.2) and (4.13), the friction factor can be written as

$$f_w = 2\kappa^2\xi_0\left|\mathbf{F}_{Mod}(\xi_0)\right|^2. \tag{4.16}$$

It is seen that Equation (4.13) is an explicit expression for the shear velocity, whose solution must be obtained iteratively. In the case of laboratory experiments, where the energy dissipation is measured, the procedure can be summarized as follows:

1. Given initial guesses for k_N and f_w, z_0, l and ξ_0 are evaluated.

2. Then, Equation (4.14) is used to obtain $\mathbf{F}_{Mod}(\xi_0)$, which in turn is substituted into Equation (4.16) to get f_w.

3. From Equation (4.15), φ_t is computed and the energy dissipation factor is then obtained from $f_e = f_w \cos\varphi_t$.

4. This value of f_e is compared to the energy dissipation factor obtained from measurements, $f_{e,exp}$.

The procedure is repeated until the desired approximation is reached. For that, the new friction factor is obtained from $f_w = f_{e,exp}/\cos\varphi_t$ and the bottom roughness from $k_N/30 = z_0 = l\xi_0$, where ξ_0 and l are obtained from Equations (4.16) and (4.7), respectively.

4.2 Velocity Profile Prediction

The velocity profile prediction using Equation (4.10) is identical to the prediction from the classical GM model, except for the fact that the profile is shifted down by a distance z_0. The modified velocity profile can be seen in Figure 4-1. The input parameters for the models are shown in Table 2.1 and in addition the friction factor and the bottom roughness are shown in Table 4.1.

Table 4.1: Bottom roughness k_N, obtained from Mathisen's (1993) and Barrantes' (1996) experiments, using the Modified GM model.

Exp.	a	b	c	d	e	f	m	n	o	PWO[a]
f_w	0.371	0.276	0.223	0.444	0.363	0.329	0.183	0.154	0.116	0.349
k_N (cm)	25.2	19.6	15.1	23.5	22.8	21.0	7.2	7.0	4.7	27.0

[a]: Barrantes (1996) experiment.

Looking to Figures 3-3 and 4-1, and specifically to the classical GM and the Modified GM models' velocity profile predictions for this particular experiment, i.e., Mathisen's (1993) Experiment "a", we can say that the new model gives a better prediction for $z < z_0$, and that the overall form of both the velocity amplitude and the velocity phase are in better agreement with Mathisen's measurements.

Now, the Modified GM model and the Constant eddy viscosity model seem, from a qualitative view, to give similar predictions of the velocity profile. A comparison between them has to be made carefully, in order to highlight relative advantages and disadvantages of the two models.

4.2.1 Comparison of the Velocity Profile Predictions

For the Constant Eddy Viscosity Model, Figure 4-1 shows that the velocity amplitude overshoot, found in the experimental data for the measurements between 2.5 and 5 cm above the bed, is relatively well described. On one hand, both the location of the lower part of the predicted overshoot and the prediction of the height at which

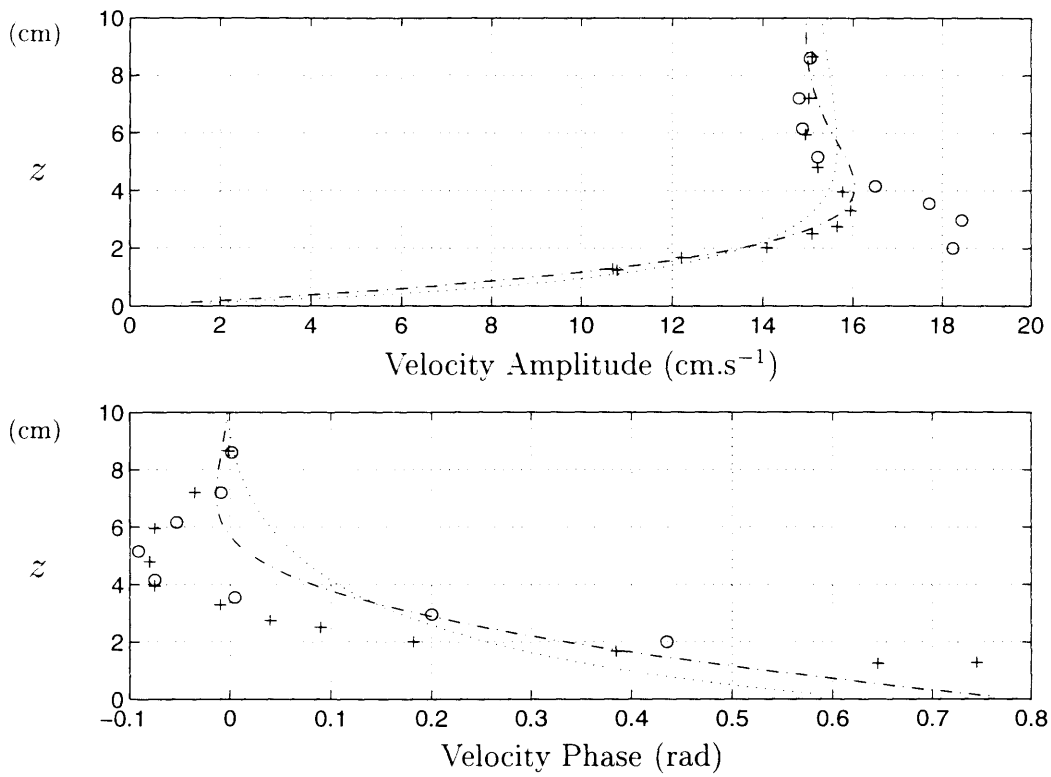

Figure 4-1: Velocity profiles obtained from 1) the Modified Grant-Madsen eddy viscosity model (*dotted line*), 2) the Constant eddy viscosity model presented in Chapter 3 (*dash-dotted line*), and 3) Mathisen's Experiment "a" measurements above the trough of the ripples (*pluses*) and above the crest of the ripples (*circles*).

the velocity is maximum fall only slightly above the corresponding measured values. Moreover, the predicted maximum velocity amplitude is in very good agreement with the experimental data. On the other hand, the upper part of the predicted overshoot extends further from the bottom than the measured values. However, the vertical shift of the predicted curve relative to the measurements remains practically constant throughout this upper part of the overshoot, meaning that the shape of this section is also well described by the Constant ν_t model.

In addition, the predicted approach of the overshoot to the outer velocity u_b is in good agreement with the measurements . Indeed, the trough measurements show that the velocity at $z = 6$ cm corresponds approximately to the outer velocity, while the Constant ν_t model's prediction shows that this velocity is reached at $z \approx 7.5$ cm.

The figure also shows that the predicted profile using the Constant ν_t model is in very good agreement with the lower measurement values.

The Modified GM Model presents a relatively weak overshoot prediction. In fact, there is a section of the predicted velocity amplitude profile where the velocity is greater than the outer velocity. However, the form of this overshoot is significantly smoother than the form obtained from the measurements. This produces that the predicted height for which the velocity is maximum and the predicted height for which the outer velocity is reached do not agree with the values obtained from the measurements.

In terms of the phase angle φ_t, none of the two models is in very good agreement with the measurements. However, Figure 4-1 shows that the Constant eddy viscosity model follows better the general trend of the experimental data points. Indeed, the high phase values found experimentally in the lower zone of the boundary layer are relatively well predicted by this model. Besides, the measurements show what could be called a phase undershoot, which is a feature exhibited more by the Constant eddy viscosity model, although to a lesser extent.

Given this behavior of the two models, it would appear that the Constant eddy viscosity model predicts the details of the velocity profile better than does the Modified GM model. This conclusion is based on comparison with a single experiment. However, in Appendix A are shown comparisons with the other pure wave velocity profiles obtained by Mathisen (1993), from which similar conclusions can be drawn.

4.2.2 Comparison of Boundary Layer Thickness Predictions

The boundary layer thickness is one of the most important features that a model should predict and a good model's velocity profile should contain the information needed to define it with a reasonable accuracy. As mentioned before, the classical Grant-Madsen model fails to predict accurately this parameter, when dealing with large roughness elements. This has been solved by artificially increasing the boundary

layer thickness, as in Mathisen and Madsen (1996).

In addition to the velocity profile itself, Figure 4-1 also highlights the existence of a well-defined boundary layer thickness, δ. Indeed, according to the experimental data shown in the figure, the bottom boundary layer has a thickness of approximately 6 cm. This value corresponds to the height, above the overshoot, at which the velocity is the closest to u_b, i.e., the elevation just after the end of the overshoot and before the velocity starts to increase, as predicted by linear wave theory. In column II of Table 4.2 are shown the estimates of the boundary layer thickness obtained visually from the experimental velocity amplitude profiles shown in Figure 4-1 and in the figures of Appendix A. Unfortunately only one of them corresponds to an experiment with 20 cm roughness spacing, Experiment "n", where partial measurements were done, allowing a rough estimation of what could have been the top of the boundary layer.

Since there is no standard way of defining the predicted δ from a particular model, we are limited to compare the models using consistent but subjective criteria.

On one hand, the scale of the boundary layer thickness for the Modified GM model can be defined, as in Grant and Madsen (1986), by

$$\delta_{Mod} = \mathcal{A}\, l = \mathcal{A}\, \frac{\kappa u_*}{\omega}, \tag{4.17}$$

where l is the parameter used to define ξ in Equation (4.8) and $\mathcal{A}$ is a scaling constant. Grant and Madsen (1986) suggest $1 < \mathcal{A} < 2$ and here, initially, $\mathcal{A} = 2$ will be used. For the Constant eddy viscosity model the scale of the boundary layer thickness is given by

$$\delta_{\nu_t = cte} = \mathcal{B} \sqrt{\frac{2\nu_t}{\omega}}, \tag{4.18}$$

where $\mathcal{B}$ is another scaling constant, which will also be set tentatively to 2. The estimates of the boundary layer thickness using Equations (4.17) and (4.18), with $\mathcal{A} = \mathcal{B} = 2$, are shown in Table 4.2 (columns III and IV). Comparing these results

with the estimates of the boundary layer thickness from the measurements, also shown in the table, we can say that the values of δ_{Mod} and $\delta_{\nu_t=cte}$, for $\mathcal{A} = \mathcal{B} = 2$, are two to three times smaller than the observed values of the boundary layer thickness. This suggests that, when dealing with large roughness elements, the value of $\mathcal{A}$ in Equation (4.17) should be higher than the value proposed by Grant and Madsen (1986), and that the validity of setting $\mathcal{B} = 2$ should also be studied.

On the other hand, a numerical scheme can be used to estimate more rigorously the values of $\mathcal{A}$ and $\mathcal{B}$ to be used when dealing with large roughness elements. Indeed, the boundary layer thickness given by Equations (4.17) and (4.18) can also be defined as the height above the bottom at which the deficit velocity amplitude $|u_d|$ becomes smaller than a prescribed fraction of the free stream velocity u_b.

For the Constant eddy viscosity model this approximation is defined as the value of z for which

$$\left| -\mathrm{e}^{\frac{-(1+i)z}{\sqrt{2\nu_t/\omega}}} \right| = \mathrm{e}^{-\frac{z}{\sqrt{2\nu_t/\omega}}} \leq \begin{cases} 1\,\% \\ 5\,\% \\ 10\,\% \end{cases} . \tag{4.19}$$

Since the results from this equation correspond to the estimations of the boundary layer thickness, z can be substituted by Equation (4.18), and Equation (4.19) becomes

$$\mathrm{e}^{-\mathcal{B}} \leq \begin{cases} 1\,\% & \text{or } \mathcal{B} \geq 4.6 \\ 5\,\% & \text{or } \mathcal{B} \geq 3.0 \\ 10\,\% & \text{or } \mathcal{B} \geq 2.3 \end{cases} . \tag{4.20}$$

This values of $\mathcal{B}$ can then be used to obtain δ from Equation (4.18). Since the eddy viscosity for this model is a linear function of $\eta^4/(\lambda^2 T)$, given by Equation (3.4), the prediction of the boundary layer thickness will only be a function of the ripple dimensions η and λ and not of any flow parameter, as shown in Table 4.2. Even if this is in some way unrealistic since we would intuitively expect the boundary layer thickness to be some function of the flow, it is consistent with the idea of using

fixed ripples while varying flow parameters. In other words, real movable ripples are sensitive to flow variations and transform accordingly, producing changes to the boundary layer thickness, while fixed ripples do not translate the flow variations into boundary layer thickness changes. It can be seen from these results that the measured values of the boundary layer thickness (column `II`) lie between the 1 % and the 5 % results using the numerical scheme. In fact, except for Experiment "a", the 1 % results are closer to the measurements than the 5 % results.

For the Modified GM model, a similar approach is taken, leading to

$$\left| \frac{\mathrm{Ker}\,(2\sqrt{\xi}) + \mathrm{iKei}\,(2\sqrt{\xi})}{\mathrm{Ker}\,(2\sqrt{\xi_0}) + \mathrm{iKei}\,(2\sqrt{\xi_0})} \right| \leq \begin{cases} 1\,\% \\ 5\,\% \\ 10\,\% \end{cases} . \tag{4.21}$$

with which the value of ξ, and then the value of z corresponding to δ, can be obtained for a given ξ_0. From that, and using Equation (4.17), the value of $\mathcal{A}$ can be estimated. These results are also shown in Table 4.2.

When dealing with the Modified GM model, it can be seen that while the 1 % approach predictions of δ are far above the experimental measurements ($\delta_{GM,1\,\%} \simeq 2\delta_{exp.}$), the 5 % approach predictions are in relative good agreement with the measurements.

Comparing the predictions from each model, shown in Table 4.2 (columns `V-XII`), it can be seen that, as said before, the 1 % approach is appropriate when using the Constant eddy viscosity model, while the 5 % approach is the best for the Modified GM model. This suggests that the decision on which model's predictions are in better agreement with the measurements will depend on the approach used in the numerical scheme. However, it can also be seen that the variability in the predictions of δ when using one approach or the other is smaller for the Constant ν_t model than for the Modified GM model. Therefore, the subjective and arbitrary choice of a specific value for the numerical approach seems not to be so crucial when using the Constant ν_t

Table 4.2: Boundary layer thickness predictions using the Constant ν_t model and the Modified GM model. All the values are in cm.

Exp.	Experimental δ	Scale δ_{Mod} ($\mathcal{A}=2$)	Scale $\delta_{\nu_t=cte}$ ($\mathcal{B}=2$)	Modified GM model 1% $\mathcal{A}$	Modified GM model 1% δ	Modified GM model 5% $\mathcal{A}$	Modified GM model 5% δ	Const. ν_t model[a] 1% $\mathcal{B}$	Const. ν_t model[a] 1% δ	Const. ν_t model[a] 5% $\mathcal{B}$	Const. ν_t model[a] 5% δ
I	II	III	IV	V	VI	VII	VIII	IX	X	XI	XII
a	6.0	2.22	3.40	12.7	13.4	6.2	6.54	4.6	7.85	3.0	5.11
b	7.2	2.50	3.40	11.6	13.63	5.5	6.50	4.6	7.85	3.0	5.11
c	7.0	2.52	3.40	10.9	12.87	5.1	6.02	4.6	7.85	3.0	5.11
d	—	1.68	3.40	13.4	10.64	6.7	5.29	4.6	7.85	3.0	5.11
e	—	2.06	3.40	12.6	12.32	6.2	6.02	4.6	7.85	3.0	5.11
f	—	2.14	3.40	12.3	12.35	5.9	5.99	4.6	7.85	3.0	5.11
m[b]	—	1.54	1.70	10.3	7.42	4.7	3.41	4.6	3.93	3.0	2.56
n[b]	3.5[c]	1.90	1.70	9.8	8.66	4.4	3.91	4.6	3.93	3.0	2.56
o[b]	—	1.90	1.70	9.0	7.99	4.0	3.50	4.6	3.93	3.0	2.56
PWO[d]	7.3	2.56	3.40	12.5	15.09	6.1	7.35	4.6	7.85	3.0	5.11

[a]: ν_t from Equation (3.4)
[b]: Experiments with $\lambda = 20$ cm.
[c]: Rough estimation from incomplete measurements.
[d]: Barrantes (1996) experiment.

model.

It is important to point out that, since the solution of Equation (4.21) can be written as $\xi = (\delta + z_0)/l = \mathcal{A} + \xi_0$, the value of $\mathcal{A}$ is a function of ξ_0 or, in terms of A_b/k_N

$$\mathcal{A} = \mathcal{A}(\xi_0) = \mathcal{A}\left(\frac{1}{6\sqrt{2f_w}(A_b/k_N)}\right). \tag{4.22}$$

With the knowledge of the bottom roughness and the friction factor, obtained with the closure procedure (Section 4.1), $\mathcal{A}$ can be plotted against A_b/k_N, as shown in Figure 4-2.

While Grant and Madsen (1986) found $1 < \mathcal{A} < 2$ for large values of A_b/k_N, which is shown in the figure to be an adequate range for $5 < A_b/k_N < 10^2$ when using the 10% approach and for $10^2 < A_b/k_N < 10^4$ with the 5% approach, it is clear that $\mathcal{A}$ increases as A_b/k_N gets smaller, i.e., as the bottom roughness gets larger. In other words, the constant $\mathcal{A}$ can safely be chosen between 1 and 2 for small roughnesses but its value has to be higher when dealing with larger roughnesses, as in the case of

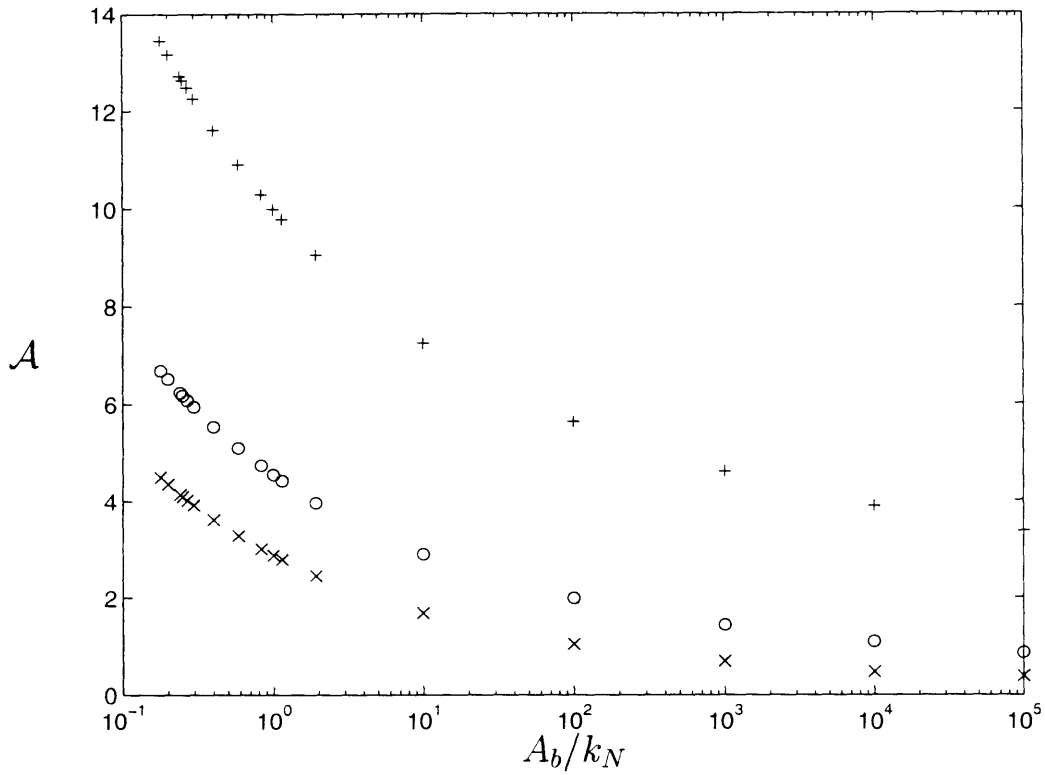

Figure 4-2: Constant $\mathcal{A}$, from Equation (4.17), as a function of A_b/k_N, for different approximations of $|u_d|$ to u_b: 1) 1% of u_b (*pluses*), 2) 5% of u_b (*circles*), and 3) 10% of u_b (*crosses*).

rippled beds. Therefore, since the shear velocity u_* is also an increasing function of the roughness, the boundary layer thickness δ cannot be considered a linear function of the boundary layer scale l, at least when dealing with flows over large roughness elements. A summary of the data plotted in Figure 4-2 is shown in Table 4.3.

Table 4.3: Constant $\mathcal{A}$, from Equation (4.17), as a function of A_b/k_N, for different approximations of $|u_d|$ to u_b.

A_b/k_N	0.2	1	10	10^2	10^3	10^4	10^5
$\mathcal{A}_{1\%}$	13.17	9.99	7.23	5.62	4.59	3.88	3.36
$\mathcal{A}_{5,\%}$	6.51	4.54	2.89	1.98	1.44	1.09	0.86
$\mathcal{A}_{10,\%}$	4.34	2.87	1.68	1.04	0.69	0.47	0.38

Finally, after the velocity amplitude, velocity phase and boundary layer thickness

comparisons, the overall conclusion in terms of the detailed velocity profile prediction is that the Constant ν_t model's results are in better agreement with the measurements than the Modified GM model.

Actually, the Modified Grant-Madsen model fails to predict a well defined overshoot and a clear end of the boundary layer. However, before discarding the idea of an eddy viscosity which varies linearly with the elevation above the bottom, an attempt to understand the poor agreement between this model's velocity profile prediction and the measurements should be made. In that sense, it is clear that the continued growth of ν_t for $z \to \infty$ represents an unrealistic feature in both the classical GM model and the Modified GM model, since by definition the turbulence is virtually zero above the boundary layer. This in turn supports the idea of a constant eddy viscosity above a certain height from the bottom. Therefore, another model should be studied, namely a combined model, where first the eddy viscosity varies linearly with depth, in a lower layer, and then remains constant above that level.

Chapter 5

Combined Model

As seen before, it is well known that the turbulence vanishes gradually with height above the bottom. In that sense, the idea of a constant eddy viscosity after a certain height above the bottom can be of interest. Therefore, a model which eliminates the unrealistic growth of the eddy viscosity as $z \to \infty$ will be derived, as a combination of the Constant eddy viscosity model presented in Chapter 3 and the Modified Grant-Madsen model presented in Chapter 4, and its performance in terms of the velocity profile prediction will be addressed. The eddy viscosity for this model is defined, similarly to Madsen and Wikramanayake (1991), as shown below.

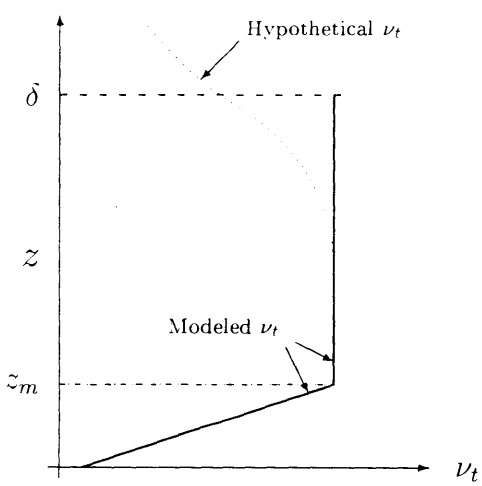

Combined model's eddy viscosity.

$$\nu_t = \begin{cases} \kappa u_*(z + z_0), & z \leq z_m \\ \kappa u_*(z_m + z_0), & z \geq z_m \end{cases} \tag{5.1}$$

where

$$z_m = \alpha_m \frac{\kappa u_*}{\omega}, \quad \alpha_m = \text{constant}. \tag{5.2}$$

5.1 Theoretical Formulation

The governing equation in this case is the same as Equation (1.17), i.e.,

$$\frac{\partial}{\partial t}(\tilde{u}_d) = \frac{\partial}{\partial z}\left\{\nu_t \frac{\partial \tilde{u}_d}{\partial z}\right\}, \tag{5.3}$$

where $\tilde{u}_d$ is the deficit velocity defined in Section 4.1. Since the definition of the eddy viscosity is not the same for the lower and upper parts of the boundary layer, the analysis has to be made for each part separately, and the solution has to match at the interface.

A. $z \leq z_m$.

In this portion Equation (4.8) still holds and the general solution reads

$$u_{d_-} = \mathtt{A}\left[\mathrm{Ker}\,(2\sqrt{\xi}) + i\mathrm{Kei}\,(2\sqrt{\xi})\right] + \mathtt{B}\left[\mathrm{Ber}\,(2\sqrt{\xi}) + i\mathrm{Bei}\,(2\sqrt{\xi})\right], \tag{5.4}$$

where $\mathtt{A}$ and $\mathtt{B}$ are constants to be determined with the boundary conditions.

B. $z \geq z_m$.

Now, substituting the definition of the eddy viscosity for this portion into Equation (5.3), we get

$$\frac{i}{\xi_m} u_d = \frac{\partial^2 u_d}{\partial \xi^2}, \tag{5.5}$$

where ξ_m is defined as

$$\xi_m = \frac{z_m + z_0}{l}. \tag{5.6}$$

The general solution for this equation is

$$u_{d_+} = \mathtt{C}\,\mathrm{e}^{\frac{1+i}{\sqrt{2\xi_m}}\xi} + \mathtt{D}\,\mathrm{e}^{-\frac{1+i}{\sqrt{2\xi_m}}\xi}, \tag{5.7}$$

where $\mathtt{C}$ and $\mathtt{D}$ are other constants to be determined.

The boundary and matching conditions for this system are

$$u_{d-} = -u_b, \quad \text{at} \quad z = 0 \quad \text{or} \quad \xi = \xi_0 = z_0/l, \qquad (a)$$

$$u_{d+} = 0, \quad \text{as} \quad z \to \infty \quad \text{or} \quad \xi \to \infty, \qquad (b)$$

$$u_{d-} = u_{d+}, \quad \text{at} \quad z = z_m \quad \text{or} \quad \xi = \xi_m = \alpha_m + \xi_0, \qquad (c)$$

$$\frac{\partial u_{d-}}{\partial z} = \frac{\partial u_{d+}}{\partial z}, \quad \text{at} \quad z = z_m \quad \text{or} \quad \xi = \xi_m = \alpha_m + \xi_0, \qquad (d)$$

Now, applying the boundary condition (a) in Equation (5.4) we get

$$\mathtt{A}\,\mathrm{K}_0 + \mathtt{B}\,\beta_0 = -u_b, \tag{5.8}$$

where

$$\mathrm{K}_\mathrm{i} = \mathrm{Ker}\,(2\sqrt{\xi_\mathrm{i}}) + i\mathrm{Kei}\,(2\sqrt{\xi_\mathrm{i}}), \quad \text{and} \quad \beta_i = \mathrm{Ber}\,(2\sqrt{\xi_\mathrm{i}}) + i\mathrm{Bei}\,(2\sqrt{\xi_\mathrm{i}}).$$

Applying the boundary condition (b) in Equation (5.7) we get simply

$$\mathtt{C} = 0. \tag{5.9}$$

Then, applying (c) and (d) in Equations (5.4) and (5.7) we get

$$\mathtt{A}\,\mathrm{K}_m + \mathtt{B}\,\beta_m = \mathtt{D}\,\mathrm{e}^{-(1+i)\sqrt{\frac{\xi_m}{2}}}, \tag{5.10}$$

and

$$\mathtt{A}\,\mathrm{K}'_m + \mathtt{B}\,\beta'_m = -\mathtt{D}\,\sqrt{i}\,\mathrm{e}^{-(1+i)\sqrt{\frac{\xi_m}{2}}}, \tag{5.11}$$

respectively, where

$$\mathrm{K}'_\mathrm{i} = \mathrm{Ker}'\,(2\sqrt{\xi_\mathrm{i}}) + i\mathrm{Kei}'\,(2\sqrt{\xi_\mathrm{i}}), \quad \text{and} \quad \beta'_\mathrm{i} = \mathrm{Ber}'\,(2\sqrt{\xi_\mathrm{i}}) + i\mathrm{Bei}'\,(2\sqrt{\xi_\mathrm{i}}).$$

and Ker', Kei', Ber' and Bei' are the first derivatives with respect to the argument of the Kelvin functions of zeroth order, which can be evaluated with polynomial approximations from Abramowitz and Stegun (1972, pp 384-385). Solving for the constants A, B and D in Equations (5.8), (5.10) and (5.11), leads to

$$\mathtt{A} = u_b \frac{\beta_m \sqrt{i} + \beta'_m}{\beta_0 \left(\kappa_m \sqrt{i} + \kappa'_m\right) - \kappa_0 \left(\beta_m \sqrt{i} + \beta'_m\right)}, \tag{5.12}$$

$$\mathtt{B} = -u_b \frac{\kappa_m \sqrt{i} + \kappa'_m}{\beta_0 \left(\kappa_m \sqrt{i} + \kappa'_m\right) - \kappa_0 \left(\beta_m \sqrt{i} + \beta'_m\right)}, \tag{5.13}$$

$$\mathtt{D} = u_b \frac{\kappa_m \left(\beta_m \sqrt{i} + \beta'_m\right) - \beta_m \left(\kappa_m \sqrt{i} + \kappa'_m\right)}{\beta_0 \left(\kappa_m \sqrt{i} + \kappa'_m\right) - \kappa_0 \left(\beta_m \sqrt{i} + \beta'_m\right)}. \tag{5.14}$$

5.2 Closure

In order to evaluate Equations (5.12) to (5.14), it is first necessary to specify the value of α_m.

Given the definition of the Combined model, its prediction of the velocity profile will always lie between the corresponding prediction from the Modified GM model and the prediction from a Constant eddy viscosity model in which ν_t depends on the choice of α_m. Indeed, for a large α_m the Combined model will tend to the Modified GM model, and for a small α_m z_m will be small and the Combined model will tend to a Constant eddy viscosity model. On one hand the choice of α_m will determine the thickness of each portion of the model and on the other hand will determine the magnitude of the constant eddy viscosity in the upper portion. Ideally, the value of α_m has to be big enough to produce a non-negligible lower portion and, at the same time, has to give a constant eddy viscosity similar to the result obtained in Chapter 3.

As seen in Figure 5-1, for small values of α_m the profile will tend to the Constant eddy viscosity model's profile and for large values of α_m it will approximate the Modified GM model's profile. The figure shows that for $\alpha_m = 0.5$ or smaller, the Combined model is similar to the Constant eddy viscosity model, in terms of the

velocity profile. This is indeed what we want since the conclusion from Chapter 4 was that the Constant eddy viscosity model gives a better prediction of the velocity profile than does the Modified GM model. Besides, given the values of the parameter l shown in Table 4.2, the value of α_m should not be too small, in order to avoid z_m to be also very small, which would suggest the use of the simpler Constant ν_t model instead of the more complicated Combined model. Following the recommendation of

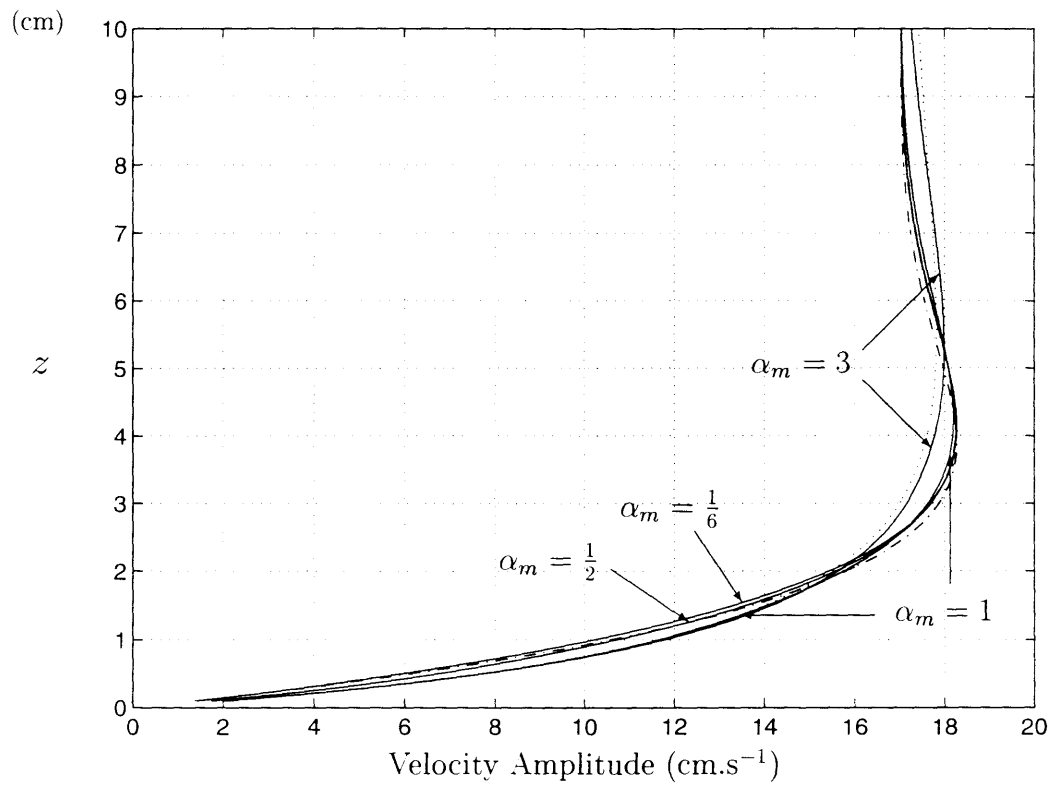

Figure 5-1: Velocity amplitude profiles obtained from 1) the Constant eddy viscosity model presented in Chapter 3 (*dash-dotted line*), 2) the Modified Grant-Madsen eddy viscosity model presented in Chapter 4(*dotted line*), 3) the Combined eddy viscosity model presented here, for different values of α_m (*solid lines*).

Madsen and Wikramanayake (1991), the value of α_m was finally chosen to be

$$\alpha_m = 0.5. \tag{5.15}$$

With this value, the magnitude of the constant eddy viscosity for the combined

model ($\nu_t = \kappa u_*(z_m + z_0)$) is similar to the magnitude of the eddy viscosity used in the Constant ν_t model ($\nu_t = \nu_{t_0}\eta^4/(\lambda^2 T)$).

Now, with $\alpha_m = 0.5$ specified, f_w and k_N have to be obtained to close the problem, similarly to the Modified GM model. Following the same approach as in Section 4.1, Equation (4.13) takes the form

$$u_* = \kappa\sqrt{\xi_0}\,|\mathbf{F}_{Comb}(\xi_0)|\,, \tag{5.16}$$

where

$$\mathbf{F}_{Comb}(\xi_0) = \mathtt{A}\mathrm{K}_0' + \mathtt{B}\beta_0'. \tag{5.17}$$

The phase angle φ_t becomes

$$\varphi_t = \arctan\left(\frac{\Im m\ [\mathbf{F}_{Comb}(\xi_0)]}{\Re e\ [\mathbf{F}_{Comb}(\xi_0)]}\right), \tag{5.18}$$

and the friction factor f_w reads

$$f_w = \frac{2\kappa^2\xi_0}{u_b^2}\,|\mathbf{F}_{Comb}(\xi_0)|^2\,. \tag{5.19}$$

The same iterative procedure as for the Modified GM model is then used, and the results are shown in Table 5.1. It should be noticed that both f_w and k_N vary from one model to the other, for a given experimental f_e.

Table 5.1: Bottom roughness k_N, obtained from Mathisen's (1993) and Barrantes' (1996) experiments, using the Combined model.

Exp.	a	b	c	d	e	f	m	n	o	PWO[a]
f_w	0.403	0.299	0.240	0.496	0.394	0.357	0.197	0.164	0.123	0.379
k_N (cm)	30.6	23.3	17.5	30.2	27.7	25.2	8.1	7.7	5.0	32.6

[a]: Barrantes (1996) experiment.

By comparing Table 4.1 to Table 5.1 it can be seen that while f_w only varies 8% on average between the two models, the variation of k_N is significantly higher, 15%

on average, reaching 22% for Experiment "d".

Finally, the solution for the velocity is complete and is given by Equations (5.4) and (5.7), where A, B, C and D are given by Equations (5.12), (5.13), (5.9), and (5.14), respectively.

5.3 Velocity Profile and Boundary Layer Thickness Predictions

In Figure 5-2 are plotted Mathisen's (1993) Experiment "a" measurements and the corresponding velocity profile predictions from each of the three models. For this

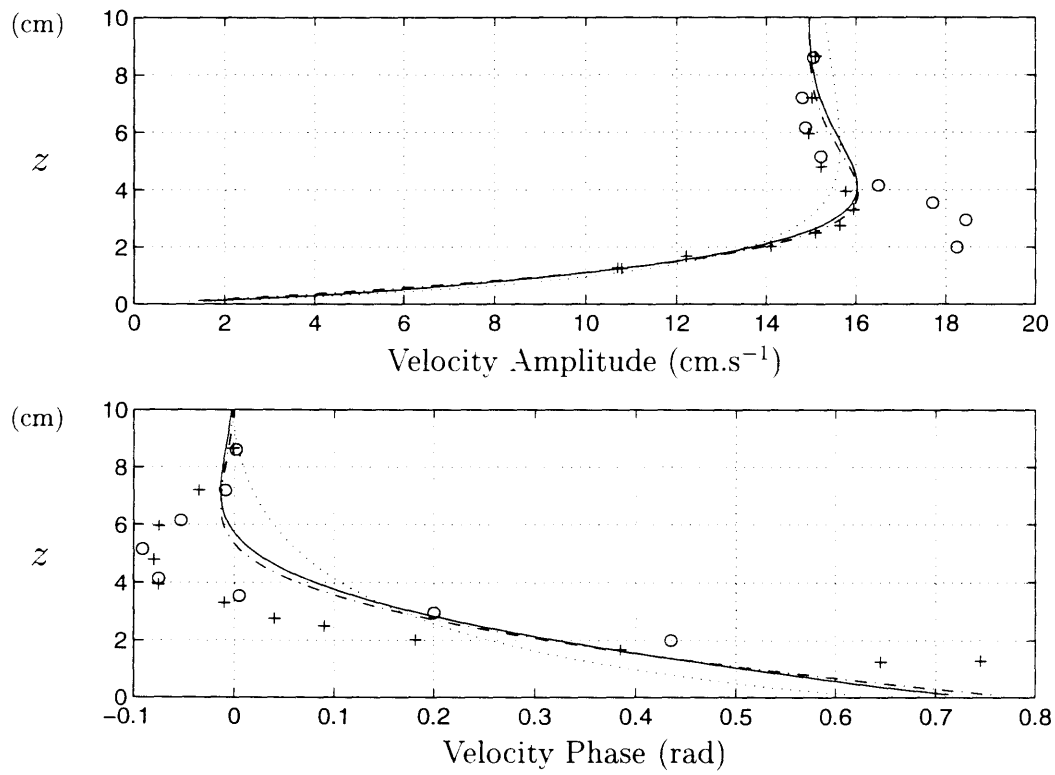

Figure 5-2: Velocity profiles obtained from 1) the Constant eddy viscosity model presented in Chapter 3 (*dash-dotted line*), 2) the Modified Grant-Madsen eddy viscosity model presented in Chapter 4(*dotted line*), 3) the Combined eddy viscosity model presented here, with $\alpha_m = 0.5$ (*solid line*) and, 4) Mathisen's Experiment "a" measurements above the trough of the ripples (*pluses*) and above the crest of the ripples (*circles*).

experiment, the values of the constant eddy viscosities used in the Constant ν_t model and in the Combined model are of the same order: 4.07 $cm^2.s^{-1}$ and 4.80 $cm^2.s^{-1}$, respectively. The other experimental results from Mathisen (1993) and Barrantes (1996), with the corresponding predictions, are shown in Appendix A.

Figure 5-2 shows that the velocity amplitude profiles from the Combined model and the Constant ν_t model are almost identical in the lower part of the boundary layer. Above that, we can see that in the overshoot the Combined model is slightly above the Constant ν_t model. Similar behavior can be seen in the other figures of Appendix A.

In general terms, we can say the main features of the predicted velocity profiles using the Constant eddy viscosity model are maintained with the Combined model.

Considering the prediction of the boundary layer thickness, δ_{Comb} can first be defined as

$$\delta_{Comb} = \mathcal{C}\,\frac{\kappa u_*}{\omega}. \tag{5.20}$$

In addition, using the same numerical scheme as in Section 4.2, δ_{Comb} can be defined as the value of z for which

$$\left| \mathrm{D}\,\mathrm{e}^{\sqrt{\frac{i}{\xi_m}}\xi} \right| \leq \begin{cases} 1\,\% \\ 5\,\% \\ 10\,\% \end{cases}, \tag{5.21}$$

where ξ and ξ_m are given by Equations (4.6) and (5.6), respectively. The results are shown in Table 5.2.

This table shows first that, similarly to the analysis of the Modified model's ability to predict the boundary layer thickness, the parameter $\mathcal{C}$, used to evaluate δ from the knowledge of the boundary layer scale l, cannot be considered constant as the relative roughness A_b/k_N varies.

Additionally, it can be seen that the magnitude of the available boundary layer thickness measurements lie between the 1 % and the 5 % approximations of both

Table 5.2: Boundary layer thickness predictions using the Constant ν_t model and the Combined model. All the values are in cm.

Exp.	Experimental	Combined model				Const. ν_t model[a]			
		1 %		5 %		1 %		5 %	
	δ	$\mathcal{C}$	δ	$\mathcal{C}$	δ	$\mathcal{B}$	δ	$\mathcal{B}$	δ
I	II	III	IV	V	VI	VII	VIII	IX	X
a	6.0	7.7	8.40	5.0	5.43	4.6	7.85	3.0	5.11
b	7.2	6.8	8.30	4.4	5.33	4.6	7.85	3.0	5.11
c	7.0	6.2	7.66	4.0	4.91	4.6	7.85	3.0	5.11
d	—	8.4	7.04	5.5	4.56	4.6	7.85	3.0	5.11
e	—	7.6	7.74	4.9	5.00	4.6	7.85	3.0	5.11
f	—	7.3	7.67	4.7	4.94	4.6	7.85	3.0	5.11
m[b]	—	5.8	4.34	3.7	2.77	4.6	3.93	3.0	2.56
n[b]	3.5[c]	5.5	5.02	3.5	3.18	4.6	3.93	3.0	2.56
o[b]	—	5.0	4.57	3.2	2.86	4.6	3.93	3.0	2.56
PWO[d]	7.3	7.5	9.53	4.8	6.09	4.6	7.85	3.0	5.11

[a]: ν_t from Equation (3.4)
[b]: Experiments with $\lambda = 20$ cm.
[c]: Rough estimation from incomplete measurements.
[d]: Barrantes (1996) experiment.

models. For the Combined model the 5 % approximation seems to be in slightly better agreement with the measurements than the 1 % approximation, and the opposite is true for the Constant ν_t model. If we chose the 1 % approximation the Constant ν_t model's prediction of δ is the best in 4 out of 5 experiments and if we choose the 5 % approximation the Combined model's results are the best, also in 4 out of 5 experiments. In fact, a 3 % and a 2 % approximations would be the best for the Combined and the Constant ν_t models, respectively. However, given the arbitrariness of the choice of a specific approximation, we can say that there are no convincing arguments to say that one model is predicting the boundary layer thickness better than the other.

This suggests that other features of the models should be analyzed in detail. In fact, the models can also be used to compute a theoretical energy dissipation factor, which can then be compared with the corresponding measurements.

Chapter 6

Energy Dissipation Factor and Bottom Roughness Analysis

In the last chapter we show that both the Constant eddy viscosity model and the Combined model give a similar prediction of the velocity profile within the bottom boundary layer. A comparison in terms of other aspects of the flow-bottom interaction is therefore needed. In this chapter, an analysis of each model's prediction of the energy dissipation is performed and then an attempt is made to determine which features from each of the models contribute to a better prediction of the flow behavior close to the bed.

Indeed, the models can also be used to compute a theoretical energy dissipation factor, $f_{e,t}$, and the results can be compared to values obtained from experiments. Fortunately, this parameter of the flow-bottom interaction has been extensively measured in experiments performed by several researchers. We are going to take advantage of this by including in our discussion more experimental data than the limited results from Mathisen (1993). The new data correspond to the experiments performed by Carstens et al. (1969), Lofquist (1986), Rosengaus (1987) and Mathisen (1989). All these experiments were performed over movable bed. The data from Rosengaus and Mathisen was obtained directly from their publications, while the other data was ob-

tained from Wikramanayake and Madsen (1991). The information relevant for this work is summarized in Appendix B.

6.1 Performance of the Constant ν_t Model

For the Constant eddy viscosity model, based on the dependency of C_D on η/A_b obtained in Chapter 2 or, equivalently, on the dependency of ν_t on $\eta^4/(\lambda^2 T)$ from Chapter 3, the energy dissipation factor f_e may be expressed as a linear function of $\eta^2/(\lambda A_b)$. Indeed, from Equations (3.3) and (3.4), a theoretical f_e can be written as

$$f_{e.t} = \sqrt{\frac{180}{\pi}}\frac{\eta^2}{\lambda A_b} \simeq 7.6\frac{\eta^2}{\lambda A_b}. \tag{6.1}$$

Given the fact that both C_D and ν_t are originally obtained with the knowledge of a measured f_e, this expression can only be used to give an idea of the model's response in terms of the energy dissipation. Moreover, this expression is only valid for the fitting obtained in Figure 2-3 or in Figure 3-1, i.e., for Mathisen's (1993) data.

If we want to use other sets of data we have to recompute the relation shown in Equation (6.1) and obtain another constant of proportionality between f_e and $\eta^2/(\lambda A_b)$, which reflects the corresponding fitting. Then, the variation, if any, of such constant has to be analyzed.

Besides, it is important to say that both, Rosengaus (1987) and Mathisen (1993), did not use the concept of energy dissipation factor and assumed the phase angle φ_t to be zero. They wrote the energy dissipation in terms of the friction factor, f_w, as

$$E_d = \frac{2}{3\pi}\rho f_w u_b^3. \tag{6.2}$$

Then, using this expression along with the rate of energy dissipation for a constant eddy viscosity model, Equation (3.1), and the more general argument from Wikramanayake and Madsen (1991) that for practical purposes f_w and f_e are identical when

dealing with rippled sand beds, the expression for the eddy viscosity, Equation (3.3), becomes

$$\nu_t = \frac{16}{9\pi^3} T f_e^2 u_b^2. \tag{6.3}$$

Expressing the eddy viscosity ν_t as in Equation (3.2), a new expression for the "theoretical" f_e, valid for the movable bed data sets reads

$$f_{e,t} = \sqrt{\mathcal{C}} \frac{3}{8} \sqrt{\pi} \frac{\eta^2}{\lambda A_b}, \tag{6.4}$$

where $\mathcal{C}$ is a new constant to be found by fitting the data, as was done in Chapter 2 and Chapter 3 for Mathisen's (1993) data. This constant corresponds to the linear regression slope of ν_t as a function of $\eta^4/(\lambda^2 T)$, using Equation (6.3). The results are summarized in Table 6.1 and Figure 6-1.

Table 6.1: Values of the constant of proportionality $\mathcal{C}$ for Equation (6.4) using data from Carstens et al. (1969), Ca.; Lofquist (1986), Lo.; Rosengaus (1987), Ro.; and Mathisen (1989), Ma.

Data Used	$\mathcal{C}$	Coefficient of Determination, r^2
Ca., Lo.	68.3	0.637
Ca., Lo., Ma.	68.3	0.670
Ca., Lo., Ro., Ma.	68.3	0.696

From this table, we can see that the value of $\mathcal{C}$ does not vary when Rosengaus (1987) and Mathisen's (1989) data are added. This is due to the fact that the period of the oscillatory motion, and in particular the bottom excursion amplitude in those experiments are smaller than in Carstens et al. (1969) and Lofquist (1986) experiments. Indeed, since the fit is forced to pass through the origin, the data points close to it (see Figure 6-1) will contribute to strengthen the linear dependency. Then, Equation (6.4) can be written as

$$f_{e,t} = 5.5\frac{\eta^2}{\lambda A_b}, \tag{6.5}$$

which, compared to Equation (6.1) shows that, as expected, the energy dissipation factor is smaller for rippled movable bed than for fixed ripples, given the roundedness of the natural ripples.

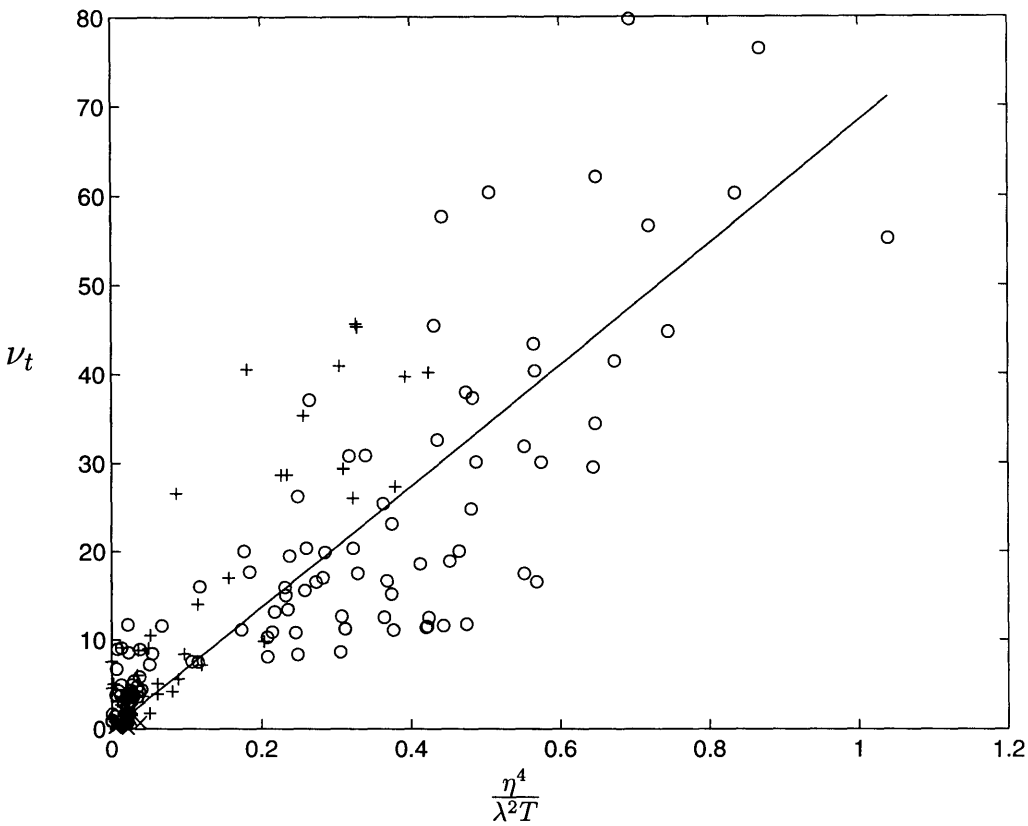

Figure 6-1: Eddy Viscosity $\nu_t = \frac{16}{9\pi^3} T f_e^2 u_b^2$ as a function of $\eta^4/(\lambda^2 T)$. Both quantities are in $(cm^2.s^{-1})$. Experimental data from Carstens et al. (1969)(*pluses*), Lofquist (1986)(*circles*), Rosengaus (1987) and Mathisen (1989)(*crosses*). The linear fitting (*solid line*) has a coefficient of determination $r^2 = 0.70$.

Now, using Equations (6.1) and (6.4), the value of the energy dissipation factor can be obtained for each of the available experiments and compared to the actual measurements. For that, the statistics used are the mean μ and the standard deviation σ of the ratio of the measured and the theoretical f_e. First, the value of $C = 68.3$ and

of $\nu_{t_0} = 180$ can be kept fixed and the mentioned statistics evaluated or, conversely, the mean of the ratio can be set to unity and the corresponding $\mathcal{C}$ and ν_{t_0} obtained, as shown in Table 6.2.

Table 6.2: Statistics of the ratio of the measured and the theoretical f_e, using fixed bed data from Mathisen (1993) and movable bed data from Carstens et al. (1969), Ca.; Lofquist (1986), Lo.; Rosengaus (1987), Ro.; and Mathisen (1989), Ma.

Data Used	ν_{t_0} or $\mathcal{C}$	μ	σ	ν_{t_0} or $\mathcal{C}$	μ	σ
Mathisen (1993)	$\nu_{t_0} = 180$	1.03	0.092	$\nu_{t_0} = 189$	1.0	0.089
Ca., Lo.	$\mathcal{C} = 68.3$	1.267	0.577	$\mathcal{C} = 110$	1.0	0.454
Ca., Lo., Ro., Ma.	$\mathcal{C} = 68.3$	1.203	0.537	$\mathcal{C} = 99.5$	1.0	0.445

It can be seen from the table that the standard deviation corresponding to Mathisen's (1993) data is much smaller than the standard deviation corresponding to the movable bed data. This is due to the fact that the coefficient of determination corresponding to the fixed bed data fitting is higher ($r^2 = 0.91$) than the one corresponding to the movable bed data ($0.63 < r^2 < 0.70$). Given that, by fixing μ to be unity, the change in ν_{t_0} (from 180 to 189) is also smaller than the changes in $\mathcal{C}$ (from 68.3 to 99.5 and 110), mostly because this model was calibrated with Mathisen's fixed bed data. In addition, it can be noticed that here again, as for the energy dissipation factor, the eddy viscosity corresponding to the sand ripples is smaller than the one for the fixed bed, which is a reasonable result.

The results of Table 6.2 will be compared with the corresponding values obtained by using the Combined model.

6.2 Performance of the Combined Model

The Combined model involves , for the portion where the eddy viscosity is not constant, the use of the bottom roughness concept. Indeed, as seen in Section 5.1, the determination of the friction factor f_w depends on the determination of the bottom

roughness k_N and both are obtained iteratively with a somewhat cumbersome procedure. Explicit formulas are also available, which express f_w as a function of k_N. Using the same functional form as in Madsen (1994) and performing a non-linear regression, as shown in Appendix C, the friction factor for the Combined model can be obtained with

$$f_w = e^{8.89\left(\frac{A_b}{k_N}\right)^{-0.059} - 10.68}, \quad \text{valid for} \quad 0.2 < \frac{A_b}{k_N} < 10^2, \tag{6.6}$$

and

$$f_w = e^{5.63\left(\frac{A_b}{k_N}\right)^{-0.106} - 7.33}, \quad \text{valid for} \quad 10^2 < \frac{A_b}{k_N} < 10^4. \tag{6.7}$$

The error associated with this expressions is very low. For Equation (6.6), the sum of squares of the differences between the exact and the approximate friction factors is 5.89 10^{-6} and for Equation (6.6) is 7.35 10^{-7}, which represent, on average, less that 0.5% of the exact value of f_w.

The energy dissipation can then be obtained from $f_e = f_w \cos\varphi_t$ where φ_t in degrees is given by

$$\varphi_t = 38.1 - 8.3 \log \frac{A_b}{k_N}, \quad \text{valid for} \quad 0.2 < \frac{A_b}{k_N} < 10^2, \tag{6.8}$$

and

$$\varphi_t = 30.6 - 4.7 \log \frac{A_b}{k_N}, \quad \text{valid for} \quad 10^2 < \frac{A_b}{k_N} < 10^4. \tag{6.9}$$

In turn, the errors associated with this two expressions are slightly bigger than the errors associated with the explicit friction factor formulas shown previously, but they only represent, on average, 3% error of the exact φ_t value. Now, in order to compare the theoretical and the measured f_e, a value of k_N has to be associated with each measured f_e. For that, k_N has to be obtained from known parameters of the flow or the bottom. Indeed, the bottom roughness has often been considered to be

proportional to the roughness height as

$$k_N = \alpha\eta. \tag{6.10}$$

For example, Grant and Madsen (1982) suggest $k_N \cong 4\eta$ for steep ripples. Here, the value of α will determine how well Equation (6.6) predicts the energy dissipation factor. This is done, as in the previous section, by analyzing the mean and the standard deviation of the ratio of the measured and the predicted energy dissipation factors. First, $\alpha = 4$ is used and the mean μ and the standard deviation σ are computed. Then, by varying α, the mean is forced to be 1, and the corresponding σ is computed.

Additionally, the same analysis is conducted by considering, as in Grant and Madsen (1982), the bottom roughness to be proportional not only to the ripple height, but also to the ripple steepness or ripple concentration, i.e., to the ratio of the ripple height over the ripple length as

$$k_N = \beta\,\eta\frac{\eta}{\lambda}. \tag{6.11}$$

The results using Equations (6.10) and (6.11) are shown in Table 6.3. From this

Table 6.3: Values of α and β and statistics of the ratio of the measured and the theoretical f_e. The data used is the fixed bed data from Mathisen (1993) and the movable bed data from Carstens et al. (1969), Ca.; Lofquist (1986), Lo.; Rosengaus (1987), Ro.; and Mathisen (1989), Ma.

Data Used	α	μ	σ	α	μ	σ	β	μ	σ
Mathisen (1993)	4	1.81	0.550	13.5	1.0	0.300	103.7	1.0	0.184
Ca., Lo.[a]	4	1.82	0.450	13.8	1.0	0.242	87.3	1.0	0.289
Ro., Ma.[b]	4	1.34	0.429	7.3	1.0	0.320	47.8	1.0	0.284
Ca., Lo., Ro., Ma.	4	1.72	0.486	12.3	1.0	0.279	78.0	1.0	0.308

[a]: wave tunnel experiments: 136 data points.
[b]: wave flume experiments: 36 data points.

table we see that, for the fixed bed data and most of the movable bed data, the best

values for α are more than three times higher than the value of $\alpha = 4$, suggested by Grant and Madsen (1982), which used for that the experimental results of Bagnold (1946). This discrepancy in the magnitude of the constant α is mainly due to the differences in the theoretical friction factor when the shear stress is evaluated at $\xi \to \xi_0$ or at $\xi \to 0$. In other words, when $\xi \to 0$ is used, the corresponding roughness for a given f_w and a given A_b is much smaller than its value when $\xi \to \xi_0$ is used, implying that α has also to be small in order to get a good agreement between the data and the model.

Another important feature shown in the table is that, for the fixed bed data, the use of Equation (6.11) is more appropriate than the use of Equation (6.10) to estimate the roughness corresponding to the experimental energy dissipation factors. This is a consequence of including the ripple concentration in the analysis. Indeed, since the bottom roughness is proportional to the ripple height and the ripple concentration, and since these parameters do not vary in a given fixed bed experiment, a natural way to take into account any variation in λ, from one experiment to another, is by including in the model the ripple concentration, η/λ, as in Equation (6.11). With this equation the bottom roughness is $k_N = 23.3$ cm for $\lambda = 10$ cm and $k_N = 11.7$ cm for $\lambda = 20$ cm. In turn, with Equation (6.10) $k_N = 20.3$ cm, regardless the ripple concentration, which seems unrealistic.

In the case of the movable bed data the opposite holds, that is, expressing the bottom roughness as a linear function only of the ripple height gives slightly better overall results ($\sigma = 0.279$ versus $\sigma = 0.308$), and the inclusion of the ripple concentration does not seem to have an important effect on the fit. This suggests, as we should expect, that the ripple dimensions for a movable bed are coupled in some way, and therefore the ripple height contains information about the ripple steepness, making unnecessary the use of both to estimate k_N. In fact, this is indeed the case since the cross-correlation coefficient for η and λ is 0.92.

Comparing Table 6.2 with Table 6.3, we can say that, for the fixed bed data, the

best performance is from the Constant eddy viscosity model ($\sigma = 0.089$ versus $\sigma = 0.184$). As said before, this is in some way artificial since the Constant eddy viscosity model itself is derived and calibrated with this same data set, and therefore should be expected to perform better. Thus, for the purpose of comparing the energy dissipation factor prediction, the more meaningful and relevant data set, from a practical point of view, is the movable bed data. So, taking into account only the movable bed data, the Combined model is giving a better prediction of f_e than the Constant ν_t model ($\sigma = 0.279$ versus $\sigma = 0.445$).

It is important to point out that the values of α and β, obtained when fitting the wave flume movable bed data (Rosengaus, 1987 and Mathisen, 1989), are significantly lower than the results corresponding to the wave tunnel experiments. This implies that, even if we should expect the results to be similar, regardless the type of model used, the measured energy dissipation in a wave tunnel appears to be higher than in a wave flume, for the same range of relative roughness. This is due in part to scale differences between the two types of experiments, since the wave flume experiments were performed with relatively small amplitudes and periods of oscillation, compared to the values used in the wave tunnel experiments. Additionally, given the complexity of the general setup and in particular of the way the energy dissipation is measured in a wave tunnel, we can say that the difficulty to distinguish and separate accurately the energy dissipation due to the bedforms from the energy dissipation due to other factors can potentially be a source of energy dissipation overestimation.

In Figure 6-2 are plotted the theoretical and the measured f_e corresponding to the movable bed data, for which $k_N = 12.3\,\eta$ was used, according to the results of the analysis with all the movable bed data, shown in Table 6.3.

It can be seen that, except for some points with high f_e, the theoretical curve fits relatively well Carstens' and Lofquist's data. The data points from Rosengaus and Mathisen fall lower than the theoretical curve, since the value of α for these data should in fact be 7.3 and not 12.3. However, a unique value for α is used, which

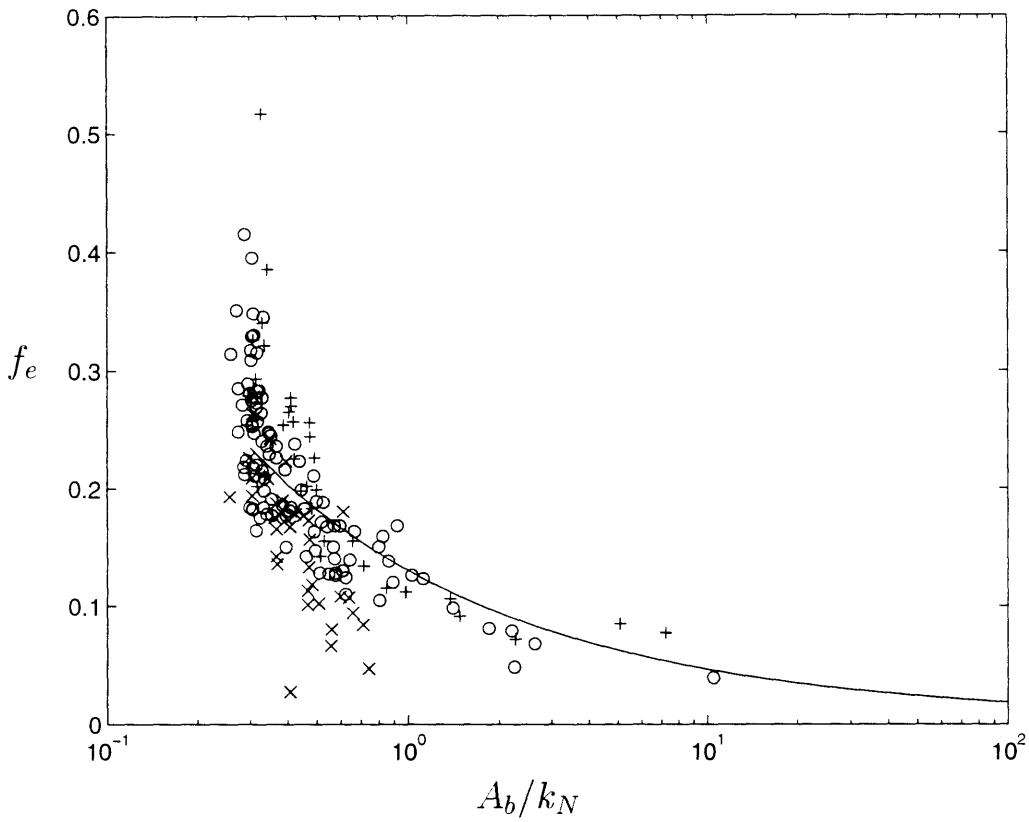

Figure 6-2: Measured and predicted energy dissipation factors, as a function of the relative roughness, A_b/k_N. Theoretical values using Equation (6.6) with $k_N = 12.3$ (*solid line*); data from Carstens et al. (1969) (*pluses*); data from Lofquist (1986) (*circles*); data from Rosengaus (1987) and Mathisen (1989) (*crosses*).

represents the overall fit.

We can finally say that, in terms of the ability to predict the energy dissipation factor, the Combined model is having a slightly better performance than the Constant eddy viscosity model.

Chapter 7

Conclusions

The present study was conducted to try to obtain an eddy viscosity model able to predict accurately the details of the velocity profile, in particular the boundary layer thickness, when dealing with pure waves over large roughness elements. Based on a drag formulation of the flow-bottom interaction, a simple relationship was obtained for the drag coefficient. From this, a constant eddy viscosity model was obtained. Then, a model based on the classical Grant-Madsen model was derived and compared to the Constant eddy viscosity model in terms of their ability to predict the velocity profile and the boundary layer thickness. Following that, another model which combines the Constant eddy viscosity model and the Modified GM model was presented and also compared to the Constant eddy viscosity model in the same terms. Finally, the Combined and the Constant eddy viscosity models were compared in terms of their capacity to predict the energy dissipation.

The drag formulation was used to express the energy dissipation in terms of the drag coefficient. This result was combined with the standard expression of the energy dissipation, which involves the energy dissipation factor, to derive an expression for the drag coefficient as a function only of the ripple dimensions and the energy dissipation factor. This expression was then used to find that the drag coefficient C_D can be expressed as a linear function of η/A_b. Given this relation, the drag model's predic-

tion of the energy dissipation became similar to that of a laminar model, suggesting the use of a constant eddy viscosity model.

The Constant eddy viscosity model is identical to the laminar model, except in the fact that the kinematic viscosity is replaced by the eddy viscosity. This approach, combined with the drag coefficient relationship found before yields to an expression for the eddy viscosity ν_t as a function of $\eta^4/(\lambda^2 T)$, which is compared to Sleath's (1991) model based on analysis of experimental results. They both share the constant eddy viscosity feature but they fail to agree on the functional form of the eddy viscosity in terms of wave and bottom parameters.

The Modified Grant-Madsen model was derived in order to have a linearly varying eddy viscosity model with a valid velocity profile prediction throughout the bottom boundary layer, which is not the case of the classical Grant-Madsen model, especially when dealing with large roughness elements. The result was a velocity profile identical to that of the classical Grant-Madsen model, but shifted down such that the no-slip condition was applied at $z = 0$, instead of at $z = z_0 = k_N/30$.

The Combined model was designed to eliminate the unrealistic continued growth of ν_t as $z \to \infty$, present in the Modified GM model. The eddy viscosity in this model was defined as linearly varying in the lower portion of the bottom boundary layer and constant in the upper part. The height at which this change occurs was determined by a constant α_m, which is also responsible for setting the magnitude of the constant eddy viscosity.

When comparing the models, their predictions of the velocity profile and the boundary layer thickness were first analyzed. It was found that the Constant eddy viscosity model's details of the velocity profile, in particular the overshoot, were in better agreement with the measurements than those of the Modified Grant-Madsen model. Then the Constant eddy viscosity model and the Combined model were compared, showing that they give similar results. Finally, the analysis of these two models' ability to predict the energy dissipation showed that the results from the

Combined model were in slightly better agreement with the measurements.

The estimation of the boundary layer thickness was done by using an expression from Grant and Madsen (1986) for the Modified Grant-Madsen and the Combined models (Equation 4.17) and its equivalent for the Constant eddy viscosity model (Equation 4.18). These equations involve constants which are not fixed *a priori*, meaning that each equation has, strictly speaking, two unknowns and therefore the determination of a theoretical boundary layer thickness cannot be made directly. Hence, these constants were evaluated by using a numerical scheme, described in Section 4.2.2, in order to obtain an estimate of the boundary layer thickness which is truly comparable with observations.

The criteria used in the numerical scheme to estimate the boundary layer thickness appeared to be consistent and rigorous for the three models, but it was not conclusive in determining which model gives better predictions of this magnitude. However, an interesting feature arose when developing this method, showing that, for the linearly varying eddy viscosity models, the boundary layer thickness δ is not a linear function of the boundary layer scale, l. Indeed, it appeared that δ is a function of the product of two monotonically increasing functions of the bottom roughness (one of them being l). This can be considered as an improvement of the boundary layer thickness modeling

In addition, when performing the energy dissipation analysis, expressions from each model for the energy dissipation factor were obtained. In the case of the Constant eddy viscosity model, the result was a simple expression involving known parameters and a constant which could be obtained by fitting the available data. At the same time, the prediction of the energy dissipation factor f_e using the Combined model implied the estimation of the bottom roughness k_N. This was done by assuming k_N to be proportional to bottom parameters. However, the determination of the constant of proportionality became a problem, and the only way to solve it was by finding the value of k_N with which the predicted f_e was in average closest to the measured f_e. Then the comparisons consisted of analyzing the variability of the

individual predictions relative to the measurements. Based on this premise, a simple expression for the bottom roughness over a rippled movable bed was found as

$$k_N = 12.3\,\eta, \tag{7.1}$$

where η is the ripple length. It is important to point out here that this expression depends on the theory used in the energy dissipation factor analysis and therefore is only valid when used with the Combined model presented in Chapter 5.

Finally, we can say that the models which are in better agreement with the measurements, in terms of the velocity profile, are the Constant eddy viscosity model and the Combined model. The first is very simple but the second presents the advantage that it predicts slightly better the energy dissipation. The choice of one or the other depends on the kind of information needed. If only an estimate of the velocity profile is needed, it can be obtained from Equation (1.8), with the knowledge of the period of oscillation, the wave amplitude, the water depth, and the ripple dimensions to evaluate the eddy viscosity given by Equation (3.4). If an estimation of the energy dissipation is desired, the Combined model is more suitable.

Appendix A

Velocity Profiles

The velocity profiles shown in this Appendix include the theoretical predictions from the Constant eddy viscosity model, the Modified Grant-Madsen model and the Combined model. Additionally the corresponding measurements from Mathisen (1993) and Barrantes (1996) are included.

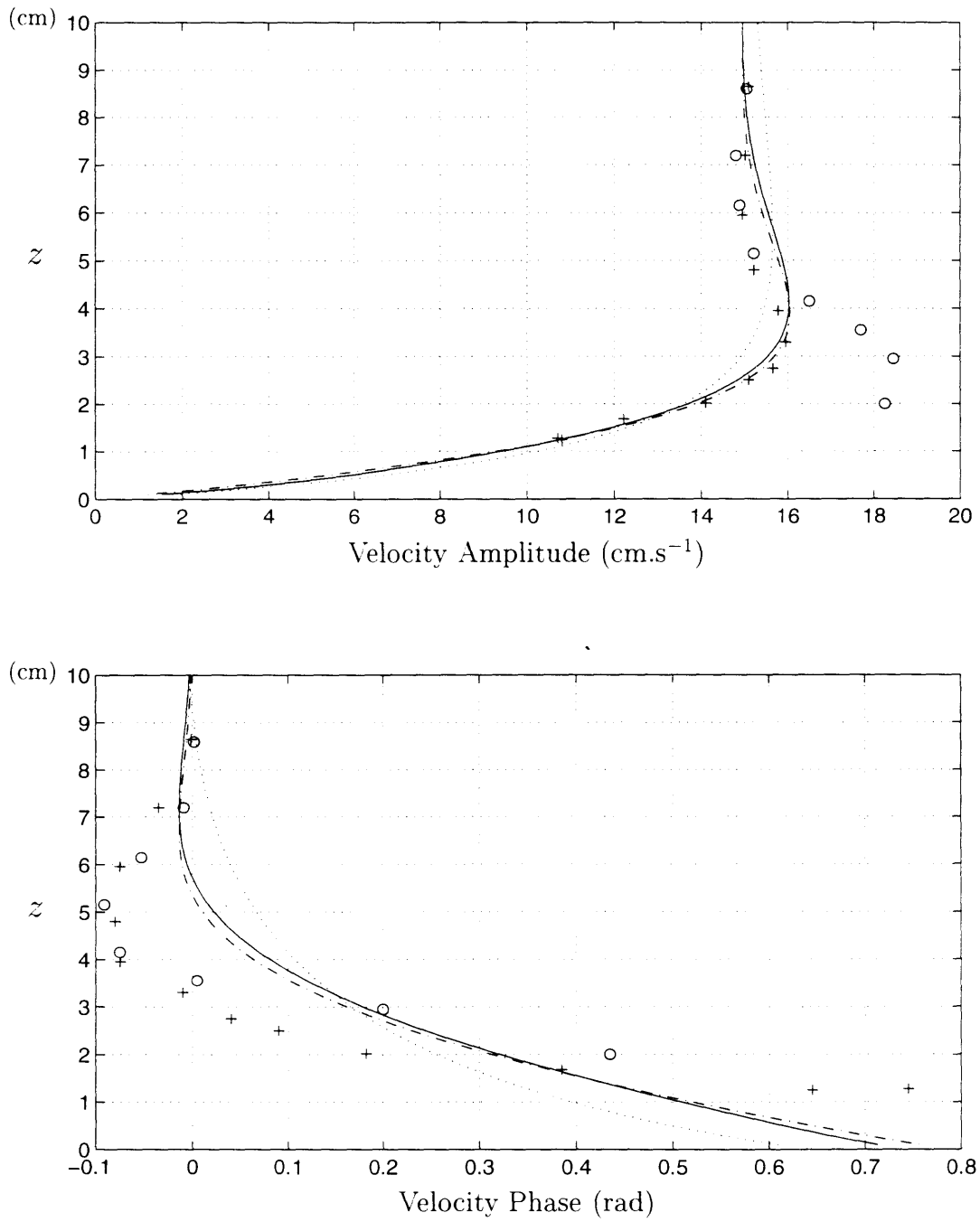

Figure A-1: Velocity profiles obtained from 1) the Constant eddy viscosity model presented in Chapter 3 (*dash-dotted line*), 2) the Modified Grant-Madsen eddy viscosity model presented in Chapter 4(*dotted line*), 3) the Combined eddy viscosity model presented here (*solid line*)and, 4) Mathisen's Experiment "a" measurements above the trough of the ripples (*pluses*) and above the crest of the ripples (*circles*).

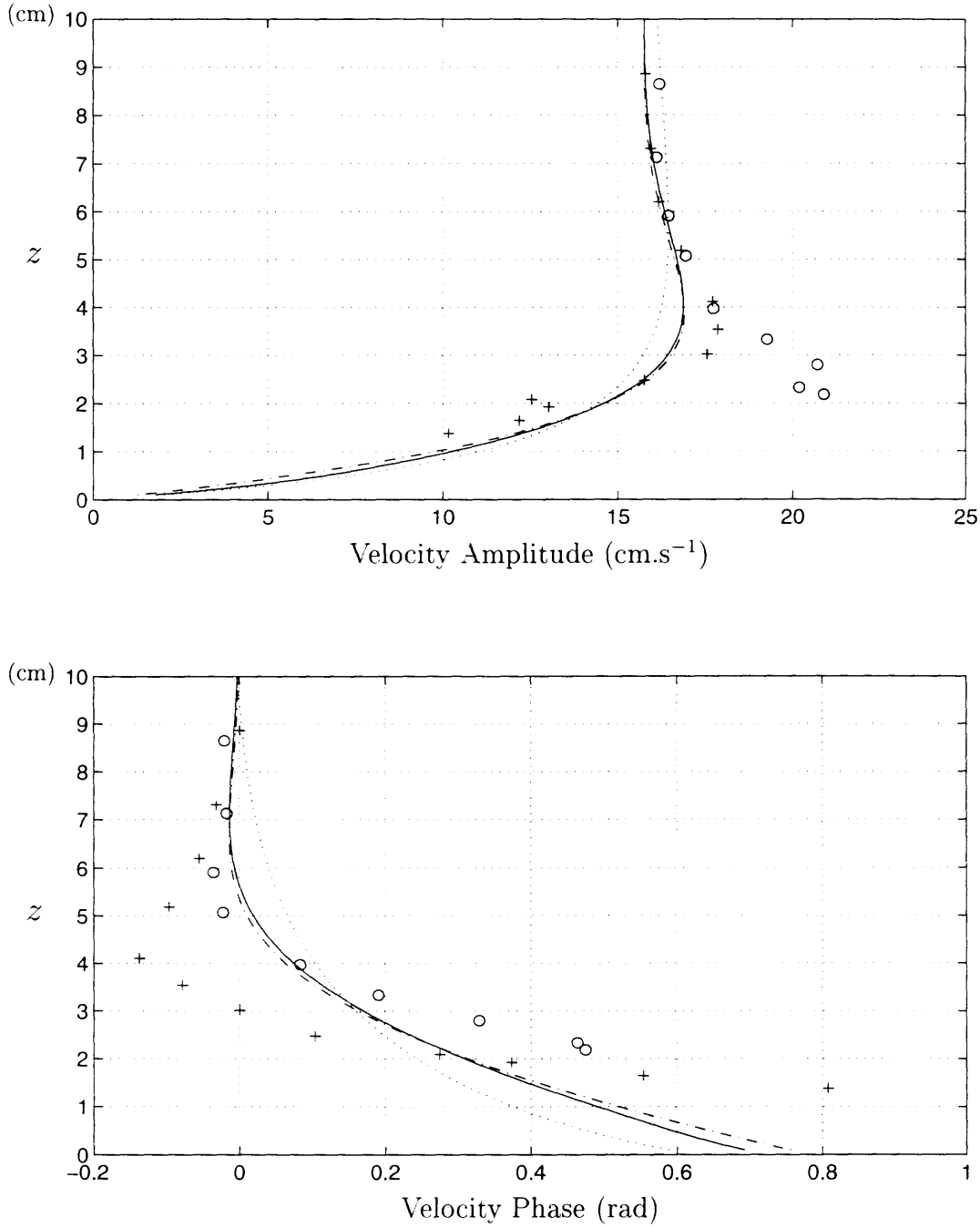

Figure A-2: Velocity profiles obtained from 1) the Constant eddy viscosity model presented in Chapter 3 (*dash-dotted line*), 2) the Modified Grant-Madsen eddy viscosity model presented in Chapter 4(*dotted line*), 3) the Combined eddy viscosity model presented here (*solid line*)and, 4) Mathisen's Experiment "b" measurements above the trough of the ripples (*pluses*) and above the crest of the ripples (*circles*).

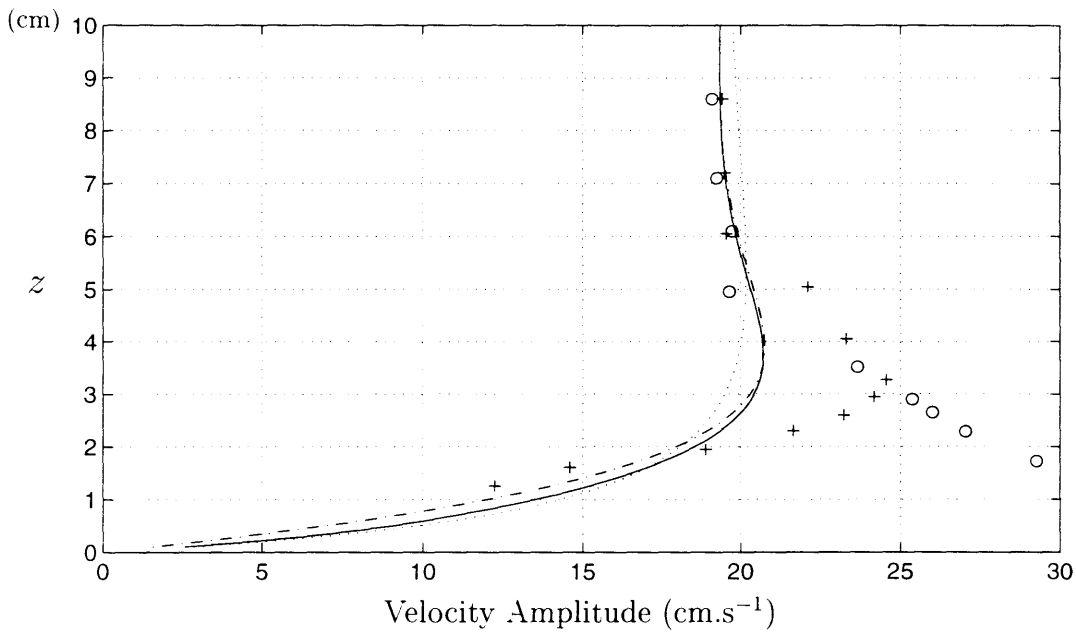

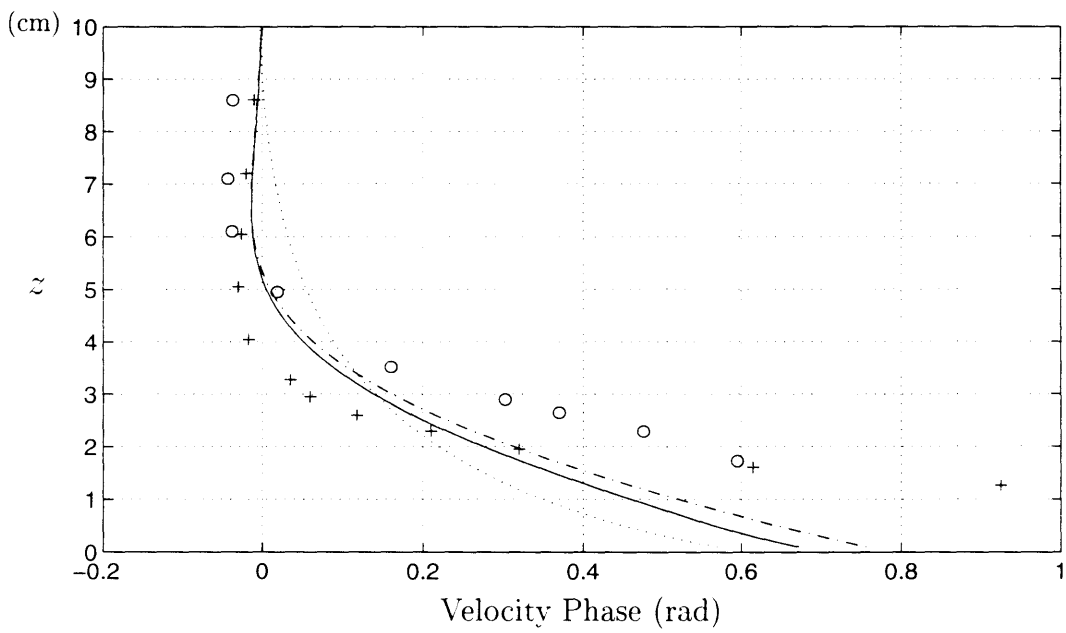

Figure A-3: Velocity profiles obtained from 1) the Constant eddy viscosity model presented in Chapter 3 (*dash-dotted line*), 2) the Modified Grant-Madsen eddy viscosity model presented in Chapter 4(*dotted line*), 3) the Combined eddy viscosity model presented here (*solid line*)and, 4) Mathisen's Experiment "c" measurements above the trough of the ripples (*pluses*) and above the crest of the ripples (*circles*).

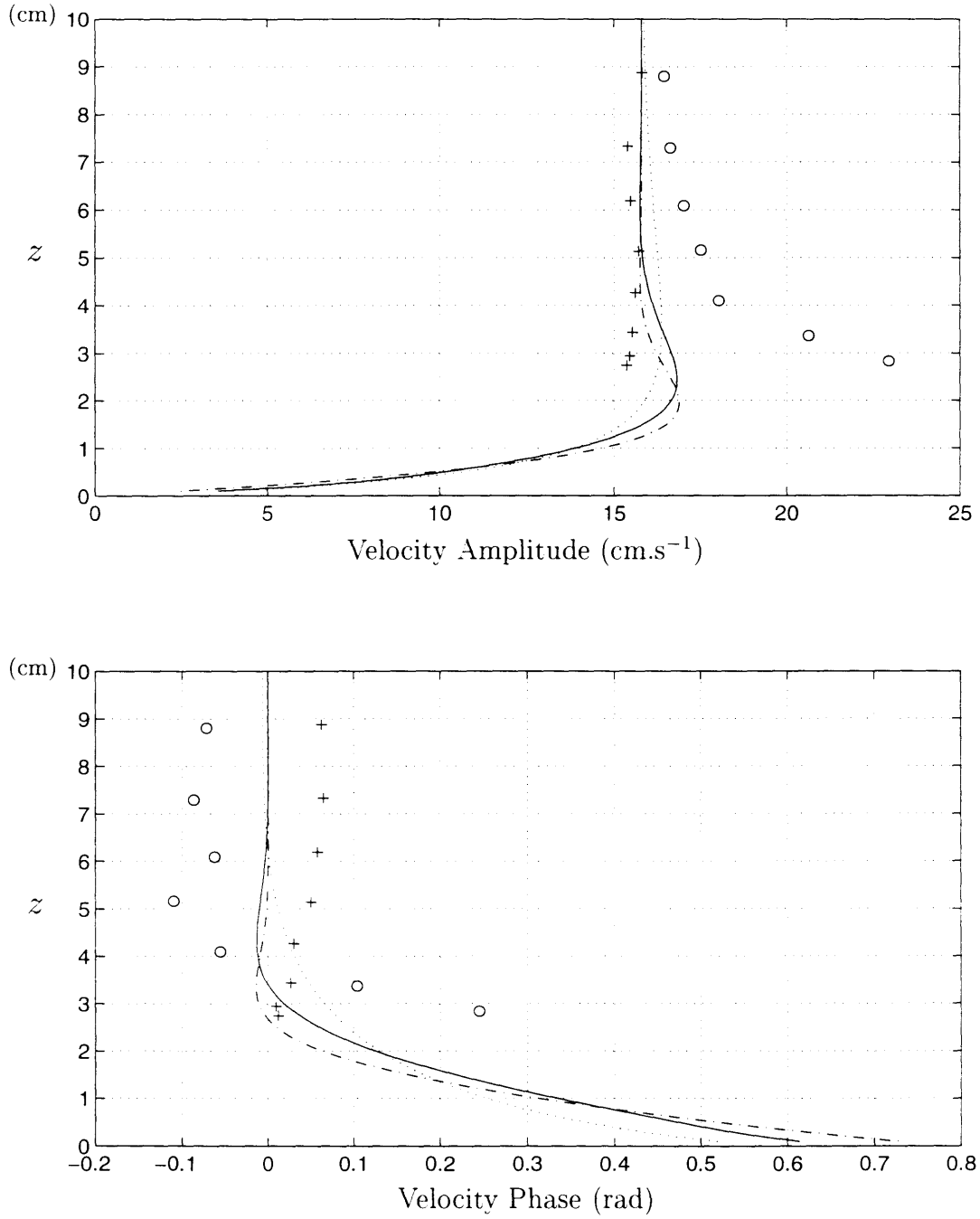

Figure A-4: Velocity profiles obtained from 1) the Constant eddy viscosity model presented in Chapter 3 (*dash-dotted line*), 2) the Modified Grant-Madsen eddy viscosity model presented in Chapter 4(*dotted line*), 3) the Combined eddy viscosity model presented here (*solid line*)and, 4) Mathisen's Experiment "n" measurements above the trough of the ripples (*pluses*) and above the crest of the ripples (*circles*).

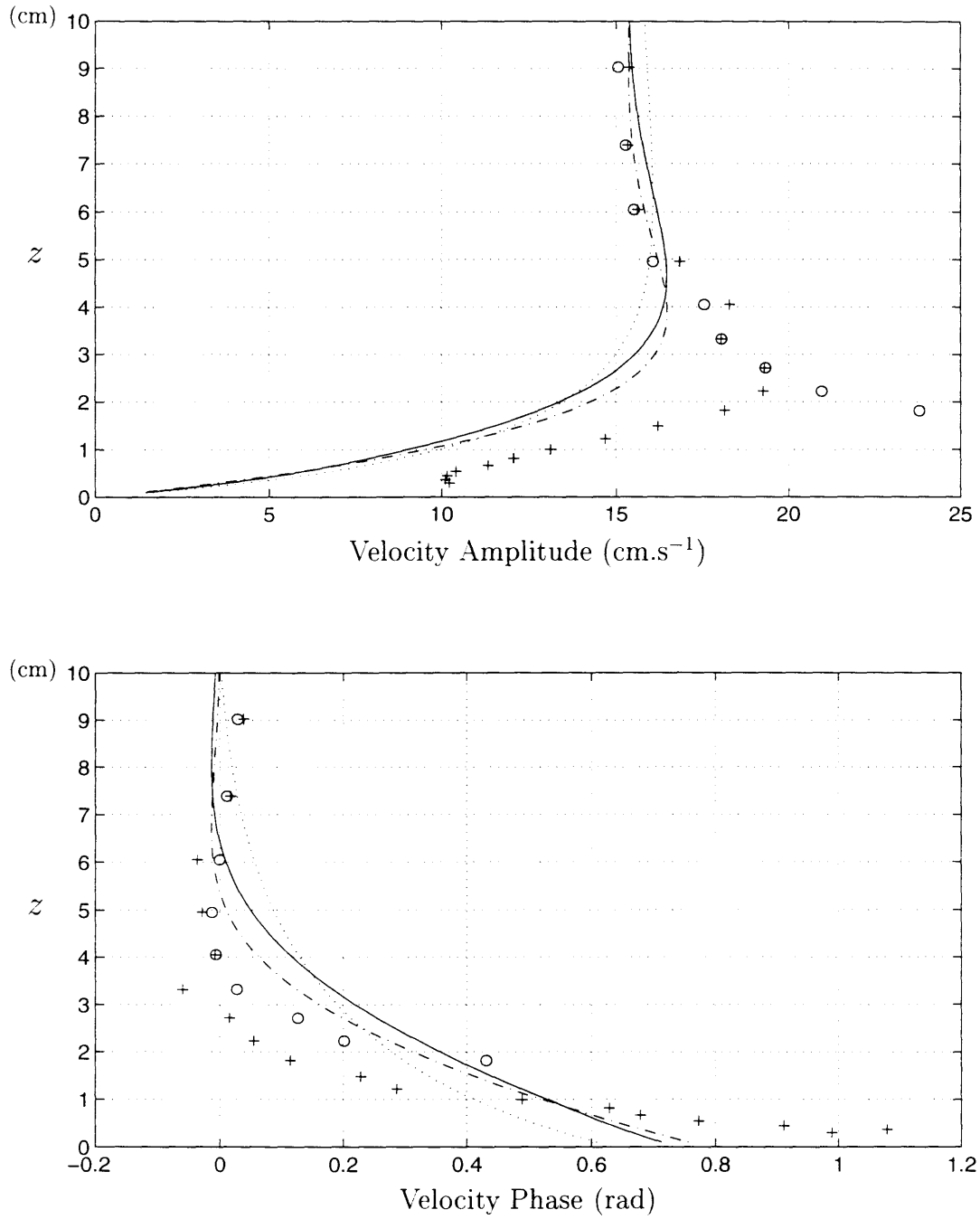

Figure A-5: Velocity profiles obtained from 1) the Constant eddy viscosity model presented in Chapter 3 (*dash-dotted line*), 2) the Modified Grant-Madsen eddy viscosity model presented in Chapter 4(*dotted line*), 3) the Combined eddy viscosity model presented here (*solid line*)and, 4) Barrantes' Experiment "PW0" measurements above the trough of the ripples (*pluses*) and above the crest of the ripples (*circles*).

Appendix B

Movable Bed Data

The movable bed data comes from Wikramanayake and Madsen (1991). Carstens et al. (1969) data come from the first experiments in which the energy dissipation over a movable bed was measured. Those experiments were performed in a wave tunnel and the energy dissipation was measured by monitoring the air pressure and the water level in the risers of the water tunnel. The data in Table B.1 is divided into three sections, corresponding to three different sandy beds: in the first section, the mean diameter is $d_{50} = 0.19mm$ and the relative density $s = 2.66$; in the second section $d_{50} = 0.297mm$ and $s = 2.47$; and in the third section $d_{50} = 0.585mm$ and $s = 2.66$.

Lofquist (1986) data also come from experiments performed in a wave tunnel. He used different types of sand and the measurements were made over equilibrium ripples as well as over growing ripples. The captions of the Tables are self explanatory.

Rosengaus (1987) and Mathisen (1989) experiments were done in a wave flume and the energy dissipation was measured by recording the change in wave height along the flume. The second section of Table B.6 and the first section of Table B.7 correspond to experiments performed with spectral waves.

Table B.1: Carstens et al. (1969).Wave tunnel data on ripple geometry and energy dissipation under regular waves.

A_b (cm)	ω (s^{-1})	λ (cm)	η (cm)	f_e
18.16	1.77	10.9	1.5	0.112
23.70	1.78	10.6	1.3	0.091
31.33	1.78	10.0	0.5	0.085
8.18	1.77	10.4	2.1	0.202
8.92	1.77	10.6	1.8	0.265
11.99	1.77	12.7	2.2	0.198
13.66	1.77	14.5	2.6	0.18
15.37	1.77	14.5	2.6	0.183
20.85	1.77	19.4	3.3	0.142
23.39	1.77	22.1	3.6	0.155
26.11	1.78	24.5	3.2	0.155
32.39	1.77	27.0	3.1	0.115
35.60	1.78	20.1	2.1	0.106
44.50	1.78	19.1	0.5	0.077
39.05	1.78	22.0	1.4	0.0717
28.08	1.77	24.5	3.2	0.134
8.00	1.76	10.4	1.9	0.385
10.11	1.76	14.6	2.8	0.254
12.01	1.77	16.7	3.3	0.279
13.77	1.77	18.1	3.4	0.340
16.07	1.77	20.4	3.9	0.321
18.54	1.78	23.9	4.5	0.211
19.65	1.76	25.2	5.2	0.326
22.35	1.77	29.0	5.8	0.293
24.19	1.77	25.7	4.8	0.277
24.77	1.78	26.4	4.9	0.270
26.64	1.78	30.0	5.6	0.254
29.08	1.77	26.2	5.0	0.256
30.80	1.76	30.4	6.0	0.257
32.68	1.77	39.1	5.6	0.244
35.18	1.78	37.8	6.8	0.225
37.43	1.77	35.7	6.2	0.226
39.22	1.81	46.3	6.9	0.202
42.35	1.77	44.1	6.9	0.199
12.45	1.78	17.4	3.1	0.517

Table B.2: Lofquist (1986). Wave tunnel data on ripple geometry and energy dissipation over equilibrium ripples with regular waves. Bed characteristics: $d_{50} = 0.18mm$ and $s = 2.65$.

A_b (cm)	ω (s^{-1})	λ (cm)	η (cm)	f_e
26.9	0.86	31.8	3.8	0.126
30.7	0.75	36.4	4.1	0.13
29.9	0.63	36.4	4.0	0.13
29.3	0.53	36.4	4.2	0.15
30.7	0.75	36.4	4.0	0.124
33.5	0.89	36.0	3.3	0.159
36.7	0.63	42.4	4.8	0.11
34.7	0.54	42.4	4.9	0.128
39.3	0.76	42.2	3.1	0.126
44.3	0.52	50.9	6.3	0.14
42.7	0.44	50.9	6.7	0.171
48.3	0.62	50.9	4.9	0.15
26.9	0.86	31.8	4	0.127
25.9	0.73	31.8	3.9	0.167
29.5	1.01	31.0	2.6	0.168
19.6	1.18	23.1	3.2	0.189
19.0	1.00	23.1	3.4	0.183
14.4	1.61	17.0	2.4	0.211
14.0	1.35	17.0	2.6	0.223
55.3	0.42	65.3	7	0.139

Table B.3: Lofquist (1986). Wave tunnel data on ripple geometry and energy dissipation over equilibrium ripples with regular waves. Bed characteristics: $d_{50} = 0.55mm$ and $s = 2.65$.

A_b (cm)	ω (s^{-1})	λ (cm)	η (cm)	f_e
23.9	1.13	31.8	7.1	0.285
23.9	1.69	31.8	6.8	0.218
23.9	1.38	31.8	7.1	0.248
31.9	1.04	42.4	8.5	0.255
25.5	1.30	31.8	6.7	0.247
22.0	1.51	31.8	6.1	0.258
20.6	1.60	31.8	5.4	0.211
27.7	1.20	34.0	6.9	0.264
17.4	1.56	23.1	4.6	0.218
17.4	1.90	23.1	4.5	0.269
17.4	2.33	23.1	4.4	0.283
17.4	2.33	23.1	4.3	0.277
31.9	1.04	42.4	8.8	0.289
31.9	0.85	42.4	8.2	0.315
23.9	1.69	31.8	6.5	0.184
25.9	2.01	31.8	5.2	0.181
28.9	2.21	31.8	4.8	0.163
23.3	1.42	31.8	6.6	0.212
23.3	1.16	31.8	6.7	0.271
23.7	1.70	31.8	6.3	0.183
25.5	2.04	31.8	5.4	0.186
28.9	2.21	31.8	5.1	0.142
17.2	1.93	23.1	4.6	0.275
17.2	1.57	23.1	4.8	0.224
17.6	2.31	23.1	4.5	0.257
24.1	1.68	31.8	6.4	0.182
25.5	1.59	31.8	6.4	0.175
22.0	1.84	31.8	5.7	0.164
20.8	1.95	31.8	5.1	0.184
27.5	1.47	31.8	6.3	0.177
31.9	1.27	43.5	8.2	0.283

Table B.4: Lofquist (1986). Continuation of Table B.3.

A_b (cm)	ω (s^{-1})	λ (cm)	η (cm)	f_e
31.9	1.63	39.5	7.9	0.240
38.3	0.71	52.2	10.1	0.348
38.3	0.87	58.0	11.5	0.351
38.3	1.06	58.0	12.0	0.314
31.1	1.68	37.3	6.9	0.236
33.9	1.88	37.3	6.2	0.199
28.3	1.43	37.3	7.3	0.220
27.9	1.18	37.3	7.2	0.277
27.5	0.98	37.3	7.1	0.273
33.9	1.54	43.5	8.4	0.215
35.1	1.49	43.5	8.2	0.247
38.7	1.65	43.5	7.7	0.184
32.3	1.25	43.5	8.6	0.253
31.9	1.03	43.5	8.6	0.317
31.9	0.85	43.5	7.8	0.345
38.3	0.86	52.2	10.3	0.309
38.3	0.70	52.2	10.2	0.395
38.7	1.05	52.2	10.5	0.281
41.9	1.25	52.2	9.8	0.229
46.3	1.38	52.2	8.9	0.238
47.9	0.69	65.3	12.6	0.330
47.9	0.56	65.3	13.5	0.415
48.3	0.84	65.3	12.9	0.329
51.9	1.01	65.3	12.2	0.248
24.3	1.65	28.1	5.8	0.178
24.3	1.35	28.9	5.9	0.198
24.3	1.11	30.3	5.8	0.236
26.7	1.95	30.2	5.5	0.150
29.5	2.17	31.2	4.7	0.128
24.3	1.63	28.8	5.6	0.191
24.3	1.63	29.0	5.9	0.209

Table B.5: Lofquist (1986). Wave tunnel data on ripple geometry and energy dissipation over growing ripples with regular waves. Bed characteristics: $d_{50} = 0.18mm$ and $s = 2.65$ for the first section of the table and $d_{50} = 0.55mm$ and $s = 2.65$ for the second section.

A_b (cm)	ω (s^{-1})	λ (cm)	η (cm)	f_e
30.7	0.76	25	2.8	0.12
30.7	0.76	26	2.9	0.138
30.7	0.76	26.7	3.1	0.105
24.3	1.63	10.3	0.75	0.068
24.3	1.63	24	4	0.147
24.3	1.63	25.7	5	0.177
30.3	1.32	14.6	1.75	0.098
30.3	1.32	24.2	3.7	0.163
30.3	1.32	32	6.3	0.216
30.3	1.32	45	7	0.245
17.6	1.32	8	0.65	0.079
17.6	1.32	13.8	2.4	0.168
17.6	1.32	21.3	3.9	0.226
38.7	1.05	7.6	0.3	0.039
38.7	1.05	12.6	1.4	0.048
38.7	1.05	15.8	1.7	0.081
38.7	1.05	21.3	2.8	0.123
38.7	1.05	36	5.5	0.168
38.7	1.05	35	6	0.188

Table B.6: Rosengaus (1987). Wave flume data on ripple geometry and energy dissipation over sandy bottom.

Exp.	A_b (cm)	ω (s^{-1})	λ (cm)	η (cm)	$f_e = f_w$	fe
N	9.082	2.39	9.90	1.570	0.1728	0.147
P	5.545	2.39	7.37	1.290	0.2425	0.206
Q	7.231	2.39	8.92	1.488	0.2230	0.189
R	12.045	2.39	10.62	1.603	0.1803	0.153
S	6.068	2.90	8.57	1.345	0.1652	0.140
T	9.157	2.03	10.16	1.598	0.1129	0.096
U	6.43	2.62	8.66	1.426	0.1874	0.159
V1	9.271	2.39	10.91	1.672	0.1766	0.150
W1	9.008	2.39	10.10	1.548	0.1564	0.133
C'	5.7737	2.30	8.68	1.520	0.2782	0.236
E'	5.312	2.39	9.09	1.450	0.2260	0.192
G'	6.6691	2.1	9.14	1.473	0.1355	0.115
X	5.5178	2.55	8.45	1.420	0.2626	0.223
Y	5.682	2.29	8.61	1.516	0.1941	0.165
Z1	7.9163	2.23	10.05	1.581	0.0275	0.023
Z2	5.4131	2.37	8.2	1.447	0.2090	0.177
A'	5.1926	2.38	7.97	1.382	0.2635	0.224
B'	5.8601	2.2302	8.21847	1.388	0.2084	0.177

Table B.7: Mathisen (1989). Wave flume data on ripple geometry and energy dissipation over sandy bottom.

Exp.	A_b (cm)	ω (s^{-1})	λ (cm)	η (cm)	$f_e = f_w$	fe
S2	4.81	2.57	7.66	1.08	0.175	0.149
S3	8.68	2.48	8.64	0.95	0.047	0.040
S5	5.92	2.38	8.45	1.183	0.167	0.142
C1	6.23	2.44	8.22	1.052	0.118	0.100
C2	6.27	2.45	7.93	1.095	0.101	0.086
D1	7.45	2.43	9.37	1.087	0.066	0.056
D2	7.63	2.42	9.11	1.111	0.08	0.068
E1	5.49	2.46	7.71	1.218	0.142	0.121
F1	6.44	2.68	8.26	1.032	0.102	0.087
F2	6.56	2.66	8.66	1.135	0.133	0.113
G1	5.91	2.65	7.56	1.210	0.174	0.148
I1	7.51	2.68	8.18	1.022	0.108	0.092
B1	4.61	2.39	6.76	1.46	0.193	0.164
B2	6.44	2.39	8.69	1.36	0.190	0.161
B3	8.00	2.39	8.83	1.02	0.107	0.091
B4	9.39	2.39	9.30	1.16	0.094	0.08
B5	10.30	2.39	9.29	1.18	0.084	0.071
B6	7.16	2.39	8.42	1.37	0.178	0.151

Appendix C

Details of the Energy Dissipation Factor Non-linear Regression

As shown in Sections 4.1 and 5.1, a bottom boundary layer model using a linearly varying eddy viscosity has the disadvantage of involving the determination of the bottom roughness and the friction factor through a somewhat complicated iterative procedure. In order to avoid this time consuming step, simple explicit formulas have been developed, which express the friction factor f_w as a function of the so-called relative roughness A_b/k_N.

For the classical GM model, Madsen (1994) suggests

$$f_w = \mathrm{e}^{7.02\left(\frac{\mathrm{A_b}}{\mathrm{k_N}}\right)^{-0.078} - 8.82}, \tag{C.1}$$

valid for $0.2 < A_b/k_N < 10^2$, which is the range of interest in our study, and then the energy dissipation can be obtained from $f_e = f_w \cos\varphi_t$ where

$$\varphi_t = 33 - 6.0 \log \frac{A_b}{k_N}, \quad \text{valid for} \quad 0.2 < \frac{\mathrm{A_b}}{\mathrm{k_N}} < 10^3. \tag{C.2}$$

These expressions are also valid for the Modified GM model. The constants in

these expressions were obtained by using known points. In particular, Equation (C.1) was obtained by fitting three points with a curve of type

$$f_w = e^{A_1\left(\frac{A_b}{k_N}\right)^{A_2}+A_3}, \tag{C.3}$$

where A_1, A_2 and A_3 are the constants to be found.

Another way of getting an explicit expression of the type of Equation (C.3) is by using a larger number of pairs $\left(\frac{A_b}{k_N}, f_w\right)$ and performing a non-linear regression. For that the Gauss-Newton method was chosen, which is based on determining in an iterative fashion the values of the constants A_i that minimize the sum of the squares of the residuals between data and nonlinear equations. The key concept underlying the technique is that a Taylor series expansion is used to express the nonlinear equation in an approximate, linear form. Following is a simplified description of the method. The details can be seen in Chapra and Canale (1990, pp 358-362).

Letting the exact friction factor be y and the approximation using Equation (C.3) be f_w, the relation between them can be expressed as

$$y_i = f_w(x_i) + e_i, \tag{C.4}$$

where $x = A_b/k_N$ and e_i is the ith error. Expanding in Taylor series and retaining only the first derivatives, the nonlinear model reads

$$f_w(x_i)_{j+1} = f_w(x_i)_j + \frac{\partial f_w(x_i)_j}{\partial A_1}\Delta A_1 + \frac{\partial f_w(x_i)_j}{\partial A_2}\Delta A_2 + \frac{\partial f_w(x_i)_j}{\partial A_3}\Delta A_3, \tag{C.5}$$

where j is the initial guess, $j+1$ is the prediction, $\Delta A_k = A_{k,j+1} - A_{k,j}$, $(k = 1, 2, 3)$. Thus, having linearized the original model, Equation (C.5) can be substituted into Equation (C.5) and we get

$$y_i - f_w(x_i)_j = \frac{\partial f_w(x_i)_j}{\partial A_1}\Delta A_1 + \frac{\partial f_w(x_i)_j}{\partial A_2}\Delta A_2 + \frac{\partial f_w(x_i)_j}{\partial A_3}\Delta A_3 + e_i, \tag{C.6}$$

or in matrix form

$$\{D\} = [Z_j]\{\Delta A\} + \{E\}, \tag{C.7}$$

where the vector $\{D\}$ contains the differences between the exact and the approximated friction factors, $[Z_j]$ is the matrix of partial derivatives of the function evaluated at the initial guess, j, the vector $\{\Delta A\}$ contains the changes in the constant values and $\{E\}$ is the vector of errors.

Applying linear least-squares theory to Equation (C.7) results in the following normal equations

$$\left[[Z_j]^T[Z_j]\right]\{\Delta A\} = [Z_j]^T\{D\}. \tag{C.8}$$

The approach consists then of solving Equation (C.8) for $\{\Delta A\}$, which can be employed to compute improved values for the constants as $A_{k,j+1} = A_{k,j} + \Delta A_k$, $(k = 1, 2, 3)$. This procedure is repeated until the solution converges, that is, until

$$|\epsilon|_k = \left|\frac{A_{k,j+1} - A_{k,j}}{A_{k,j+1}}\right|, \quad k = 1, 2, 3,$$

falls below an acceptable stopping criterion.

With this method, the values of the constants A_1, A_2 and A_3 are significantly different than in Equation (C.1), and Equation (C.3) becomes

$$f_w = \mathrm{e}^{7.94\left(\frac{A_b}{k_N}\right)^{-0.068} - 9.74}. \tag{C.9}$$

However, the errors associated with the non-linear regression and with the "three-point method" used in Madsen (1994) are of the same order. Indeed, the sum of squares of the differences between the exact and the approximate friction factors is 7.82 10^{-5} when using Equation (C.1) and 1.33 10^{-5} when using Equation (C.9), and for both equations the average error represents less than 1% of the exact value. Therefore, even if they appear to be different, Equations (C.1) and (C.9) are equivalent for the purpose of evaluating f_w or f_e with the knowledge of k_N.

Bibliography

Abramowitz, M. and Stegun, I. A. (1972). *Handbook of Mathematical Functions*, Vol. 55 of *National Bureau of Applied Mathematics Series*. Dover Publications Inc., Mineola, N.Y.

Bagnold, R. A. (1946). Interaction between waves and sand bottoms, *Proceedings of the Royal Society* **187**: 1–18.

Barrantes, A. I. (1996). *Turbulent Boundary Layer Flow over Two-Dimensional Bottom Roughness Elements*, ScD dissertation, Massachusetts Institute of Technology, Cambridge, MA.

Carstens, M. R., Neilson, F. M. and Altimbilek, H. D. (1969). Bedforms generated in the laboratory under an oscillatory flow, *Technical Report TM-28*. U. S. Army Corps of Engineers, Coastal Engineering Research Center.

Chapra, S. C. and Canale, R. P. (1990). *Numerical Methods for Engineers*. Applied Mathematics Series, McGraw-Hill International Editions, Singapore.

Devore, J. L. (1991). *Probability and Statistics for Engineering and the Sciences*, third edn. Brooks/Cole Publishing Company, Pacific Grove, CA.

E, X. and Hopfinger, E. J. (1986). On mixing accross an interface in stably stratified fluid, *Journal of Fluid Mechanics* **166**: 227–244.

Fredsøe, J. and Deigaard, R. (1992). *Mechanics of Coastal Sediment Transport*, Vol. 3 of *Advanced Series on Ocean Engineering*, World Scientific, N.J.

Grant, W. D. and Madsen, O. S. (1979). Combined wave and current interaction with a rough bottom, *Journal of Geophysical Research* **84**(C4): 1797–1808.

Grant, W. D. and Madsen, O. S. (1982). Movable bed roughness in unsteady oscillatory flow, *Journal of Geophysical Research* **87**(C1): 469–481.

Grant, W. D. and Madsen, O. S. (1986). The continental shelf bottom boundary layer, *Annual Review of Fluid Mechanics* **18**: 265–305.

Jonsson, I. G. (1966). Wave boundary layer and friction factors, *Proceedings of the 10th Conference on Coastal Engineering*, ASCE, Tokyo, Japan, pp. 127–148.

Kajiura, K. (1968). A model of the bottom boundary layer in water waves, *Bulletin of the EarthQuake Research Institute* **46**: 75–123.

Le Méhauté, B. (1976). *An Introduction to Hydrodynamics and Water Waves*, Springer-Verlag, New York.

Lofquist, K. E. B. (1986). Drag on naturally rippled beds under oscillatory flows, *Technical Report MP-86-13*, U. S. Army Corps of Engineers, Coastal Engineering Research Center.

Madsen, O. S. (1994). Spectral wave-current bottom boundary layer flows, *Proceedings of the 24th International Conference on Coastal Engineering*, ASCE, Kobe, Japan, pp. 384–398.

Madsen, O. S. and Wikramanayake, P. N. (1991). Simple models for turbulent wave-current bottom boundary layer flow, *Technical Report DRP-91-1*, U. S. Army Corps of Engineers, Coastal Engineering Research Center.

Madsen, O. S., Poon, Y.-K. and Graber, H. C. (1988). Spectral wave attenuation by bottom friction: Theory, *Proceedings of the 21st Coastal Engineering Conference*, ASCE, Costa Del Sol, Malaga, Spain, pp. 492–504.

Mathisen, P. P. (1989). *Experimental study on the response of fine sediments to wave agitation and associated wave attenuation*, MSc thesis, Massachusetts Institute of Technology, Cambridge, MA.

Mathisen, P. P. (1993). *Bottom Roughness for Wave and Current Boundary Layer Flows over a Rippled Bed*, PhD dissertation, Massachusetts Institute of Technology, Cambridge, MA.

Mathisen, P. P. and Madsen, O. S. (1996). Waves and currents over a fixed rippled bed (2), bottom and apparent roughness experienced by currents in the presence of waves, *Journal of Geophysical Research* **101**(C7): 16543–16550.

Newman, J. N. (1977). *Marine Hydrodynamics*, MIT Press, Cambridge, MA.

Nielsen, P. (1992). *Coastal Bottom Boundary Layers and Sediment Transport*, Vol. 4 of *Advanced Series on Ocean Engineering*, World Scientific, N.J.

Rosengaus, M. (1987). *Experimental Study in Wave Generated Bedforms and Resulting Wave Attenuation*, ScD dissertation, Massachusetts Institute of Technology, Cambridge, MA.

Sarpkaya, T. and Isaacson, M. (1981). *Mechanics of Wave Forces on Offshore Structures*, Van Nostrand Reinhold Co., New York, NY.

Sleath, J. F. A. (1985). Energy dissipation in oscillatory over rippled beds, *Coastal Engineering* **9**: 159–170.

Sleath, J. F. A. (1987). Turbulent oscillatory flow over rough bed, *Journal of Fluid Mechanics* **82**: 369–409.

Sleath, J. F. A. (1991). Velocities and shear stresses in wave-current flows, *Journal of Geophysical Research* **96**(C8): 15237–15244.

Wikramanayake, P. N. and Madsen, O. S. (1991). Calculation of movable bed friction factors, Technical Progress Report. Prepared for the U. S. Army Corps of Engineers, Coastal Engineering Research Center, Waterways Experiment Station.